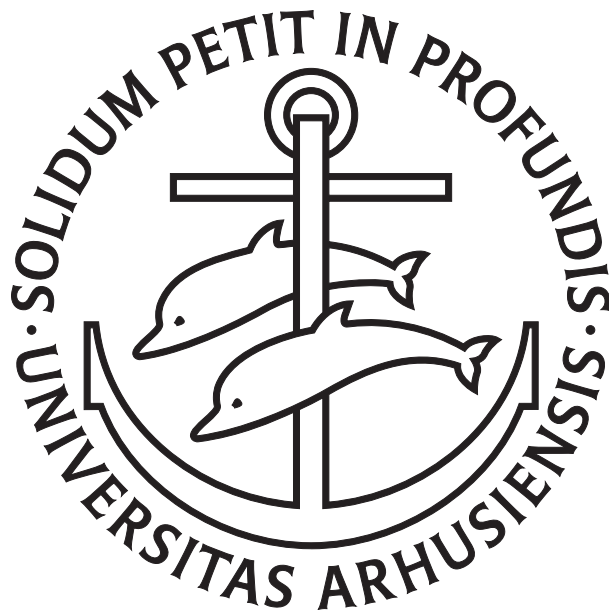# Low-energy Nuclear Reactions

Exploratory work on ^{11}Be

Hans Henrik Knudsen

Department of Physics and Astronomy
University of Aarhus

Dissertation for the degree of Doctor of Philosophy

August 2008

Hans Henrik Knudsen
1st Edition, August 2008
Department of Physics and Astronomy
University of Aarhus
Ny Munkegade, Bld. 1520
DK-8000 Aarhus C
Denmark
Phone: +45 8942 1111
Fax: +45 8612 0740
Email: hhk@phys.au.dk

I swear, by my life and my love of it,
that I will never live for the sake of another man,
nor ask another man to live for mine.
Ayn Rand (1905 - 1982)

Contents

Preface

A couple of technical remarks needs to be made before we get to the actual thesis part of this - well - thesis. First of all, throughout this thesis I will be using *Pluralis Auctoris* or authors plural. This is not to be confused with *Pluralis Majestatis*, but is simply the form I find most natural when presenting research. I am also of the opinion that the inclusion the reader, you, makes for a more interesting text both when reading and writing.

The second technical point; even though I have tried to identify sources for all my figures, some have simply turned up on my laptop. Most likely they were downloaded for a talk at one point or another and the source then subsequently forgotten. Thus I claim no credit for any figures not explicitly referring to this original research, except where specified.

Outline

The topic of this thesis is low-energy nuclear reactions, specifically with low-energy radioactive ion beams, RIB. Reactions with low energy beams creates low energy particles, and detecting and identifying these can be difficult. For this reason development of a new identifying system is also covered.

The thesis has two parts. In part one we present the first exploratory study of the reaction ^{11}Be+d performed at low beam energies. This has ben done using a post accelerated ISOL beam at REX-ISOLDE at CERN. In part two we present the initial findings from the Detection of Low Energy charged Particles project, DLEP. This project aims to identify particles using Pulse Shape Analysis of the signals generated in the detector.

In chapter one an introduction to nuclear physics is given for the non-specialist, as well as a reminder of the topical issues in nuclear reactions physics. The second chapter is a thorough presentation of ISOLDE and the REX post-accelerator. Chapter three describes our experimental setup as well as the procedures used for calibration and data analysis. Special emphasis is put in the data acquisition system and other technical issues that influence detector signals. This will be used in chapter six which describes development of a Pulse Shape Analysis tool for online particle identification. Chapter four contains a preliminary analysis of the data from the low-energy reaction ^{11}Be+d performed at REX-ISOLDE. Chapter five has a preliminary analysis of the complementary reaction ^{11}Be+p performed at the same time. Chapter seven contains a summary as well as an outlook.

Acknowledgments

Many people have played an important role during my eight years of studying physics and living in Aarhus. It would be difficult to mention everyone by name in this thesis, but some certainly deserve to a place.

The following would not have been possible without my two supervisors, Karsten Riisager and Hans Fynbo, who talked me into joining their group and thus become a Nuclear Physicist.[1] I wish to thank both of you for everything that you have enabled me to do these past four years. For constructive feedback and help throughout my studies and work with this thesis. In the same spirit I would like to thank all the current and former members of our small group Christian, Oliver, Solvieg and finally Henrik from who I have inherited much computer code. Also Aksel, Dmitri, Martin and Raquel, we have had many fruitful and stimulating discussions over the years and I have certainly learned a lot from you all.

I would also like to thank our collaborators in Madrid and Gothenburg. Haakan Johansson for teaching me all that I know about DAQs. Olof and Maria for letting me join their group in Madrid for half a year. John McGrath for fun times on and of CSIC, J&J Books and Coffee for keeping me sane while in Spain and Miguel and Martin for many fun hours of physics and beer drinking, not necessarily at the same time.

I would like to thank Karsten Handrup for helping me with the front page very close to the deadline. Nikolaj Zinner deserves great credit for proof reading the final thesis and for many interesting discussions over the years.[2]

Casper Henriksen should be thanked for many things, but most recently for keeping me company online while I was writing this thesis (from Boston, with me in Aarhus, on the same schedule). Henrik Andersen - welcome back.

This could go on forever so I resort to a list, I would like to thank the following: MF2000, ATP, TAAGEKAMMERET and everybody there, Fysisk FredagsBar, Fysikshow, Partyteam, Celia HV, Klaus Seiersen, Per Graa, Sune Riise, Soren Galatius, Thomas Lassen and Niels Buhl. You have all made my time in Aarhus a lot more enjoyable!

From the "Old days" I would like to thank Morten Bjerregaard for company the first few years up here, though you have left Aarhus I hope we will still keep in touch. Also I thank the closest I will ever come to a second brother, Rasmus Mejer, for always keeping me grounded and *not* for being faster on a bicycle.

To you all, it has been a privilege to study physics in your company and

---

[1]On a less serious note, Nuclear Physicist is right up there with Rocket Scientist on the coolness of education factor. I don't think Nuclear Physicists appreciate that enough.

[2]Yes, I'll finish that article soon...

it still is an honor to know such fantastic people as you.

Finally I would like to thank my parents and my brother for their unending support and confidence in me. You serve as my base and my safe heaven and I love you all. I would also like to mention my grand parents, though most of them are not here any more, I know how much this would have meant to them.

List of Publications

[I] H. H. Knudsen, H.O.U.Fynbo, *et al* :
β-*decay of* ^{13}O,
Phys. Rev. C **72** (2005) 044312.

Chapter 1

Introduction

This introduction is separated in two parts, each serving its own purpose. The first part is a general introduction to contemporary nuclear physics for the non-scientist. Here we try to give a very brief overview of basic nuclear physics and its applications in modern society. The hope is that this section will give the non-scientist access, if somewhat limited, to some of the other parts of this thesis and at the same time highlight the impact made by nuclear physics applications.

In the second part we present very briefly the basic nuclear physics results that will allow if not an understanding then at least an appreciation of what will follow for the non-specialist, and will server as a reminder for the rest of us.

1.1   Very basic nuclear physics

The nucleus is at the center of the atom and consist of two types of particles - protons and neutrons, commonly called nucleons. The nucleus is positively charged and has what is called a magnetic moment, meaning that if you put it in a magnetic field it will align with the field like a regular magnet. The positive charge of the nucleus comes from the charge of the protons, and both protons and neutrons have a magnetic moment that they contribute to the moment of the nucleus. For light and stable nuclei the number of protons and neutrons is similar. The number of protons in a nucleus is usually denoted Z, while the total number of protons and neutrons, also called the mass number, is denoted A. Nuclei with the same number of protons, but a different number of neutrons are called isotopes, so ^{3}He and ^{4}He are both helium isotopes, the first has only one neutron while the second has two.

Apart from the nucleus the atom also contains electrons, but for the purpose of this thesis, and nuclear physics in general, these can be ignored for two reasons. The first is distance. Electrons are very far away from the
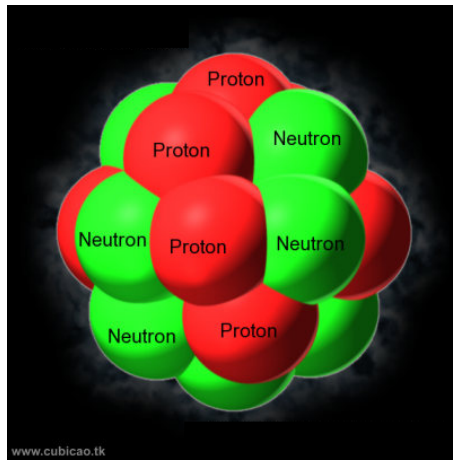
Figure 1.1: The atomic nucleus. Protons and neutrons do *not* have different colors.

nucleus. If the nucleus had a diameter of 1 cm the electrons would be 1 km away. The second is mass. The electron weighs around 1/2000'th of a proton and so a nucleus hitting an electron is the same as a grown man hitting a small bag of chips.

Since a nucleus in general contains several positively charged particles that will repel each other something else must be keeping the nucleus together. This force is called the strong nuclear force, and basically acts like glue holding the nucleus together as long as its constituents are touching each other. This gives rise to the popular model of a nucleus as balls of protons and neutrons sticking to each other, as seen in figure 1.1. Surprisingly this very simple model is not that far fetched.

If a nucleus is produced, or exists, with an overweight of either protons or neutrons it will decay, that is change its composition, to become more stable.[1] This can be done in several ways, depending on what will make the nucleus more stable. It can convert a proton to a neutron or a neutron to a proton, in both cases emitting what is called β-radiation [2], or it can emit a helium nucleus consisting of two protons and two neutrons, also called an α-particle. There are about 339 naturally occurring nuclei of which 269 are stable.

Nuclei can also be made to react with one another, thus forcing a more violent change of composition. Usually this is done by bombarding one type of nucleus onto another. This can be denoted in two ways, either with an

---

[1] In the same way that a football placed on top of a hill will roll down to the foot of the hill.

[2] Corresponding to a positron or an electron

arrow as in

$$A + B \rightarrow C + D, \tag{1.1}$$

or with the shorthand $A(B, C)D$. We will be using both notations in the following.

1.2 Contemporary uses of nuclear physics

Nuclear physics plays an important, if somewhat unrecognized[3], role in modern society. The reason for this lack of recognition is partly due to events between 1942 and 1946, and partly due to campaigns sorrounding an accident in 1986 in Ukraine. The field has never fully recovered the massive anti nuclear campaign that followed, leaving us the names sub-atomic physics and Magnetic Resonance Imaging instead of nuclear physics and Nuclear Magnetic Resonance imaging. So for that reason I will try to give a brief overview of where nuclear physics and nuclear physicists contribute to society.

The first point to mention is nuclear energy. Even though the knowledge that a nuclear chain reaction could be used to produce energy dates back to the 1940s, nuclear power is experiencing a comeback on the back of rising energy prices and growing concerns about emission of CO_2 from the burning of fossil fuels. A country like France that produces more then 98% of its electrical power from nuclear plants has one of the lowest emissions of CO_2 per capita in Europe. In the long run fusion power, which makes energy the same way as the sun, from the ITER-collaboration currently setting up shop in southern France has the potential to make an even greater impact, provided they get enough funding.[4] This, and not lack of scientific progress, has been the main obstacle for the development of fusion power to date.

Another area nuclear physics has and is making a huge contribution to is medicine. Nuclear Magnetic Resonance Imaging, MRI or just MR, is an imaging technique using the intrinsic magnetism of the nucleus [1]. This is a very used diagnostics tool e.g. for cancer victims but also used in research ranging from chemistry to medicine. Brain research in particular uses MRI extensively as a tool to probe brain function and functionality, while stroke victims benefit from new so called functional MRI able to distinguish a blood clot from a hemorrhage.[5]

Another diagnostics tool derived from nuclear physics is Positron Emission Tomography or PET [1]. In this method a patient is injected with a radioactive nucleus attached to a bio-molecule. This molecule will attach

---

[3]Sometimes even within the field.

[4]The US Congress recently canceled the American contribution of 150 million USD to this project, choosing instead to save Fermilab from budget cuts.

[5]For more information see e.g. the work performed in Aarhus by the Center of Functionally Integrative Neuroscience at www.cfin.au.dk

Figure 1.2: Ötzi the Ice-man, who lived at one of two possible lakes close to the Italian-Austrian border 5000 years ago - determined using isotope analysis

itself to e.g. a tumor or a particular active place in the brain. Measuring the decay then gives us information about the position of the biomolecule and the size of the tumor or the activity in the brain. Many nuclear physics research facilities deliver these medical radioactive nuclei to the local hospitals. The ability to manufacture these nuclei is a direct product of basic nuclear physics research. In the future perhaps tumors will be treated by attaching radioactive nuclei to them using a similar technique where the decay kills the tumor.

The last medical application we shall mention is particle therapy; treating cancer by bombarding it with radioactive particles or even anti-particles. This is a relatively new and exciting area where technology from nuclear physics research and accelerator construction is vital for success. The benefit from using particles compared to traditional x-ray (gamma) radiation is the ability to focus radiation on a much smaller area, enabling treatment of tumors very close to sensitive areas such as the eyes or parts of the central nervous system. Although a small facility at Harvard has pioneered this technique using protons since the 1960's it is not until recently that large scale treatment has become feasible due to the technological development. A test facility using carbon has been in operation at GSI in Darmstadt, Germany, since 1997. An upgraded facility is now constructed but still not commisioned in Heidelberg [2].

Turning away from medicine, another area significantly influenced by nuclear physics is the dating of archaeological artifacts using radio carbon or ^{14}C dating. In short, the radioactive isotope ^{14}C is constantly created in the atmosphere by cosmic radiation, and since all living organisms[6] are Carbon-based, as long as they are alive they exchange Carbon with the environment.

---

[6]That we know so far.

Upon death this exchange stops, and the ^{14}C will decay. Measuring the amount of ^{14}C versus stable ^{13}C that does not decay, the time of death can be established equally well for wood, fish, or humans.[7] Using accelerator and detection techniques from nuclear physics, dating can be performed very accurately using only milligrams of material [3]. The refinement of this technique, using it on other elements like Oxygen, allows determination of not only when but also where a human might have lived. One the most spectacular findings in this area is the determination of where Ötzi the Iceman, who lived around 3000BC, was born and lived his life [4].

The final area we shall highlight is security. This is a rather new, but nonetheless very important area for nuclear physicist.[8] Everything from secure disposal or re-processing of nuclear waste, decommissioning of nuclear weapons, to detection of radioactive materials in trucks or containers, fits into this category. While the research in this area is not yet significant at universities, at least in Europe, with the political focus on terrorism and the publicity this area gets, it is likely to see growth in the near future.

Finally there is of course all the contributions that nuclear physics makes to basic research in areas such as astronomy, cosmology and solid state physics, and the potential to make fundamental discoveries using nuclear physics methods. The search for neutrino-less double beta decay, which would have a big impact on very fundamental aspects of physics, is an example of this. In short, nuclear physics is far from dead, and to answer a question received at a family function recently: "Nuclear physics, don't we know all that already?", the answer is no.

With that short recap of contributions made by nuclear physics today, let us spend a few pages highlighting the important steps to how we got this far in less then a hundred years, and at the same time set the stage for the rest of the thesis.

1.3 Nuclear physics historically

Naturally, nuclear physics started with the discovery *of* the atomic nucleus.[9] This cornerstone of modern physics was seen for the first time in the famous experiment by Geiger and Marsden in 1909, showing that if you let α particles impinge on a foil of either gold or silver, some of them bounce back directly at you. This was interpreted by Lord Rutherford in 1911 to mean that the atom must have central hard and heavy core, a nucleus. Up until that moment, electrons were a well know particle from electrodynamics with quite well know properties. It was also know that atoms were formed by

---

[7]At least until the industrial revolution when combustion of fossil fuels, all containing Carbon, polluted the atmosphere enough to make this technique unusable!

[8]My guess would also be that if the marketing is done correctly, funding for this area could be very significant.

[9]In the following section much of the information is from [5] and [6].

electrons and something else having a positive charge since the atom was neutral. The specific properties of the other part however escaped contemporary scientists. A repeat of the experiment in 1913 confirmed Rutherfords theory and a new field of physics was born.

1.3.1 Nuclear Reactions

Since it was assumed that radiation, which had previously been observed, was a phenomenon produced by the nucleus and not the electrons, the idea of artificially transmuting nuclei using radiation was natural. The first transmutation, or nuclear reaction, was made by Lord Rutherford. He let α-particles hit a Nitrogen target and observed protons as a result, corresponding to the reaction

$$^{4}\text{He} + {}^{14}\text{N} \rightarrow {}^{1}\text{H} + {}^{17}\text{O}. \tag{1.2}$$
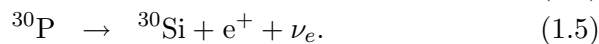
It was initially speculated that the nucleus could be formed by protons and electrons, but this theory had problems. These were solved in 1932 by Chadwicks interpretation of an experiment performed by Curie and Joliot. In 1930 Bothe and Becker had previously seen very penetrating radiation from the reaction

$$^{4}\text{He} + {}^{9}\text{Be} \rightarrow {}^{12}\text{C} + \text{n}. \tag{1.3}$$

Curie and Joliot sent the radiation through paraffin wax and saw emission of protons of too high an energy for the unknown radiation to be of the electromagnetic kind known at the time. Chadwick correctly interpreted the penetrating radiation to be a massive particle with a mass similar to the proton mass, but electrically neutral; the neutron [7].

Since the mass of nuclei were so close to an integral number of proton masses, and the neutron mass very close to the proton mass, it was reasonable to assume that a nucleus with mass A and charge Z was made up of Z protons and $(A - Z)$ neutrons. This was later shown to be exactly the case.

The discovery of the building blocks of the nucleus naturally paved the way for many new nuclear reactions. We will highlight just one; the first observation of an artificially produced radioactive nucleus made by Curie and Joliot in 1934 in the follwing reaction and its subsequent decay;

$$^{4}\text{He} + {}^{27}\text{Al} \quad \rightarrow \quad {}^{30}\text{P} + \text{n} \tag{1.4}$$
$$^{30}\text{P} \quad \rightarrow \quad {}^{30}\text{Si} + \text{e}^{+} + \nu_{e}. \tag{1.5}$$

The production of radioactive isotopes has not stopped evolving since. It is remarkable that to this day we still use the same basic tool to gain knowledge of nuclei. While the technology of course has evolved immensely during the last 70 years o fnuclear reaction physics, the production of radioactive isotopes, and most recently nuclear reactions *with* radioactive isotopes, is still our basis for probing the nuclear system.
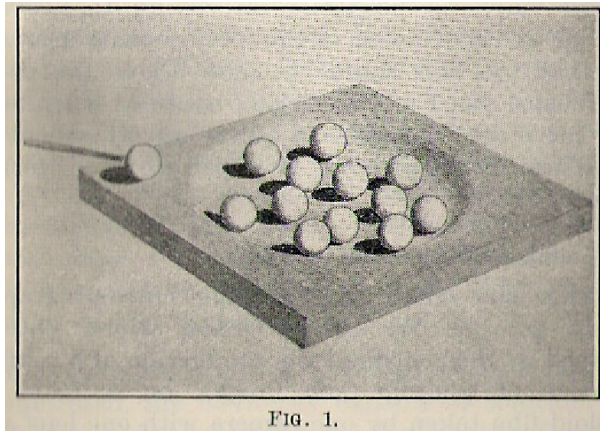
FIG. 1.

Figure 1.3: The original illustration from [8] of the compound nucleus mechanism.

1.3.2 Nuclear Structure and Models

While knowing the constituents of the nuclear system is a nice beginning, investigating their interaction and the structures they form is the next logical step. Since reactions and decays are our only probes of nuclear structure, model building has always played a very central role.

One of the first attempts to model the nuclear system was done by Niels Bohr shortly after the discovery of the neutron. Experimentally it was seen that in some reactions the emitted particle would take much longer to be emitted then the time it should take for the incoming particle to traverse the volume of the nucleus. Something was delaying the reaction, and Bohr suggested his now famous idea of the compound nucleus [8]. The idea is that the reaction between nuclei A and b has an intermediate step, C, before the emission of particles, D and e,

$$A + b \rightarrow C^* \rightarrow D + e. \tag{1.6}$$

In the intermediate step, the energy of the incoming particle is distributed among all particles in the nucleus, destroying any knowledge of how the state was created. Subsequently the energy ends up, by chance, on a single nucleon (or α-particle), which is then emitted. The idea was illustrated in Nature as using billiard balls seen in figure 1.3. Perhaps surprisingly this model was very successful, and to this day we still talk about fast reactions as direct reactions, and reactions with an intermediate step as compound reactions.

From compound nuclei we jump to the next significant development in nuclear models, which is the nuclear shell-model by Mayer and Jensen in 1949. Like the shell-model for atomic electrons, it is worth noting that the

nuclear shell-model is a mean-field model. That is, it is assumed that the force felt by a single nucleon is independent of all the specifics of the other nucleons. This is counter intuitive when thinking of the nucleus like in the primitive model in figure 1.1, where a nucleon only interacts with its nearest neighbors. Nevertheless this is a very successful model.

Like the electrons, protons and neutrons are fermions, and like the electronic shell-model the nuclear shell-model is based on the exclusion principle; each particle of a given type has to have a unique set of quantum numbers, forcing nucleons into higher energy states. Since protons and neutrons are two different particles they each have their own shell structure, giving rise to the classical illustration seen in figure 1.4. Here we see six protons and six neutrons, corresponding to ^{12}C, with two particles, one of each spin, in the first level which is called $s_{1/2g}$, the second shell, the $p_{3/2}$, fits four nucleons, and the scheme continues in a similar fashion.

The shell-model is very successful in explaining nuclear excitation energies and spin quantum numbers of these excitations, as well as the binding energy of nuclei, that is the amount of energy it takes to remove either a proton or a neutron from the nucleus. The full distribution of shells can be seen on the right hand side of figure 1.4. To the left are the basic shells and to the right the splitting of the sub-levels into different groupings is visible. This splitting is due to the spin of individual nuclear spins interacting with orbital angular momentum[10], and it gives rise to a set of Magical Numbers or shell gaps, that are marked in the figure as well. Since the distance in energy to the next level is relative much larger for magic levels, nuclei that have a magical number of nucleons in one or both shells are more tightly bound, and thus relatively more stable than neighboring nuclei. This is similar to the noble gases for atoms.

With the shell-model we can view direct reactions of the type (d,p) as adding a neutron to a particular neutron shell, while a reaction of the type (p,d) corresponds to simply removing a neutron from its shell. This interpretation of direct reactions as probing the nuclear structure is very fundamental, and as we shall see later in this thesis, as useful as ever.

While the shell-model treats each nucleon as an independent particle, and explained reaction data very nicely, collective models have had great success in describing other aspects of nuclear structure. An early collective model was built on the observation that the strong nuclear force had a very short range, so a nucleon would only interact with its nearest neighbors. This is similar to what is seen in liquids and so the liquid-drop model of nuclear behavior was suggested[8].

It might seem counter-intuitive that two such different approaches to modeling the nucleus can both be successful, but nevertheless this is the case. Modifications of the liquid drop model has been successful in explaining

---

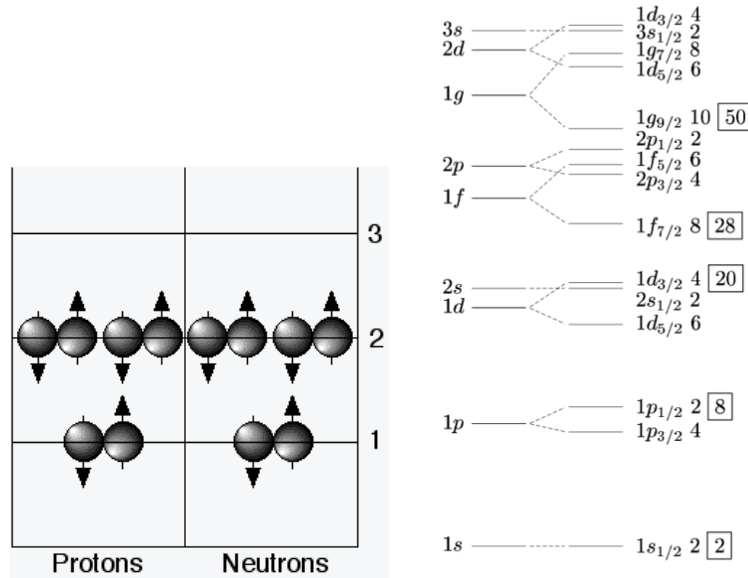[10]This is similar to what is found for electrons in atoms

Figure 1.4: Illustration of the shell-model and the magic numbers

deformation of the nucleus. Like a liquid drop, the nucleus can be deformed and subsequently rotated. The theory for nuclear deformation and rotation led to Aage Bohr and Ben Mottelson receiving the Nobel prize in 1975.

1.4 Modern nuclear physics

As already mentioned the number of proton-neutron configurations that are naturally abundant is less then 350, and all other configurations have to be created in the laboratory to be studied. Modern day nuclear physics facilities can produce over 3000 different nuclei, illustrated in the nuclear chart in figure 1.5. Currently it is estimated that up to 6000 nuclei should be bound sufficiently to allow some investigation of their structure, meaning they have a half-life of more than 1μs. The models described above, in particular the shell-model, have been very successful in explaining nuclear properties for a wide range of these nuclei. However it has become increasingly clear that for the most extreme nuclear systems, that have only been within experimental reach for the last 10-20 years, all of our current models fail.

Two features, not completely independent, show up in these extreme systems that have a disproportionate number of one type of particle. The first, seen in neutron rich nuclei, is the appearance of a neutron skin or halo around the nucleus. Put in other terms, the radius of the neutron distribution becomes significantly larger then the proton radius. This has dramatic effects on the reaction probabilities, since the outer neutrons are
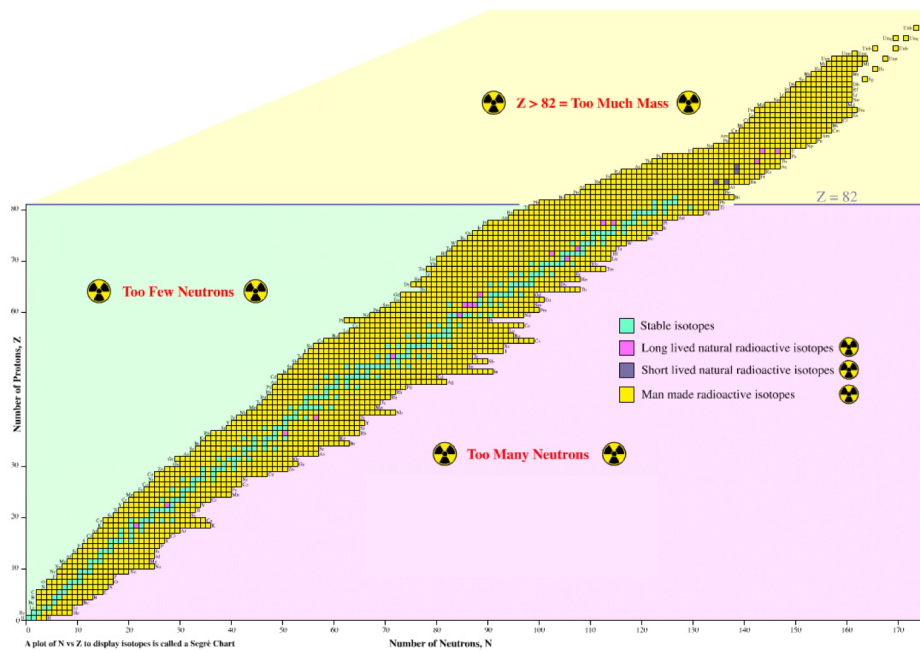
Figure 1.5: Nuclear chart showing all produced isotopes. Every square corresponds to a specific nucleus. The valley of stability is seen in blue in the middle, while everything in yellow is man made

now more easily accessible, but it also drastically changes the excitations spectrum [10].

The second effect is the disappearance of, or possibly shift in, the magic numbers discussed above. As one type of particle dominates the nucleus, the level scheme seen in figure 1.4 changes, and also these changes can be rather drastic. Disappearance of magic numbers has been seen in both intermediate mass and light nuclei and is thus a general effect associated with imbalance between protons and neutrons. Since the basic shell-model assumes that protons and neutrons are independent of each other, it is clear that in this case the model breaks down and needs to be corrected [10].

One advance that has helped our understanding of nuclear systems immensely, is the availability of raw computing power. Numerical calculations based on different models have been and are still very important tools for understanding and describing nuclear structure. They play a very important role in the understanding of experimental data and the extraction of physical parameters from it. But even though both models and computing power have developed significantly in recent times, ab initio calculations are still only possible for up to 12 particles, and then only for the stable isotope ^{12}C [9]. Calculations for other nuclei must still have some experimental input, or make some invasive assumptions, to fix model parameters.

On the experimental side we have reached a technological level where we can design a nuclei to our specifications, or at least choose a very specific nucleus to study. Several experimental facilities exists, one of them being ISOLDE which we will return to in the next chapter, where a very wide range of radioactive nuclei can be accessed at high yields and delivered to the experiment of your choice. Thus, as claimed in a recent Science article [11], we have reached the era of designer nuclei, and to be even more commercial, femtometer technology.

1.4.1 Reaction studies

The experimental techniques used to probe the structure of extreme nuclei is similar to the techniques used all the way back at the beginning of nuclear physics. Decay studies, as well as nuclear reactions at high and low energy, are still the tools of the trade, although with much better detectors, data acquisition and analysis tools,. The internal structure of an unknown nucleus is still probed by letting it interact with a nucleus with known properties and observing the results The same basic concept that was in use 70 years ago.

The difference between then and now, besides the amount of nucleons available, is the amount of control we have over the exotic nuclei. Reactions can take place with a very low energy of only a few MeV per nucleon, or MeV/u as it is usually written, and up to several hundreds of MeV/u. Thus different aspects of nuclear structure can be probed, and the same structures
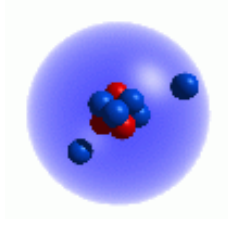
Figure 1.6: Classical illustration of the ^{11}Li double halo nucleus. The first halo nucleus to be observed.

can be probed at different energies sometimes giving unexpected results.[11] Detector technology has also developed immensely, giving us unprecedented angular and energy resolution of both emitted charged particles as well as gammas.

Compared to the classical reactions we saw earlier, several other technical differences are worth noting. Since we now study reactions of nuclei with a half-life down to the ms scale, the beam has to be unstable particle, and the known nucleus the target. Since the known nucleus is usually a very light one, typically a proton or a deutron, this means working in so-called inverse kinematics. The center-of-mass system more or less moves with the beam particle, depending on its kinetic energy. Therefore particles from the reaction will be emitted more along the beam direction, although they cover the entire angular spectrum in the center of mass system.

1.5 Light nuclei far from stability

The center of attention for this thesis is the work performed in our group in Aarhus and in the Madrid, Aarhus and Göteborg (MAGISOL) collaboration on light nuclei far from stability. In this respect light means with mass numbers lower then 20. Far from stability means with a very skewed relation between protons and neutrons, typically in favor of more neutrons since very proton rich light nuclei are unbound due to Coulomb repulsion.

These light extreme nuclei contain many of the features mentioned above that have been topical of nuclear structure research in the past decade. The neutron halo, actually a double halo of two neutrons, was first observed in ^{11}Li in 1985 by I. Tanihata and collaborators [12]. Subsewuently the effect was theoretically described in [13] which also coined the term "halo". ^{11}Li is interesting on its own for several reasons, one of them being that it is a Borromean nucleus; each of its subsystems, the ^{9}Li core and the two halo neutrons are unbound, while the entire nucleus is bound.

---

[11]See the introduction in Chapter 4

The neutron rich Beryllium isotopes also show several interesting features; ^{11}Be has a one neutron halo, while both ^{11}Be and ^{12}Be shows a disappearance of the N=8 magical number. The content of this thesis focusses on Beryllium isotopes, and we shall return to them in chapter 4.

One of the advantages of light nuclei is that the small number of particles allows for detailed modeling using numerical methods. As mentioned above, ab initio calculations can at present be performed for up to 12 particles, leaving the exotic states of light nuclei within reach of full theoretical description.

Chapter 2

ISOLDE and REX

The experiment presented in this dissertation was performed at the ISOLDE facility at CERN, Switzerland. This facility, and CERN in general, has played a pivotal role during my years as a PhD student. Through participation in a range of experiments as well as schools and other stays, a large part of my practical knowledge of experimental physics in general and nuclear physics in particular, has been acquired here. At the same time, data from experiments performed at ISOLDE, specifically REX which we shall return to below, has comprised the bulk of my analysis work. In other words, most of my PhD has revolved around CERN in one way or another. The small part that has not we shall return to in the last chapter of this thesis.

2.1   ISOLDE

The cornerstone of the low energy nuclear physics being done at CERN is the ISOLDE facility. The name is an acronym for Isotope Separator On-Line[1], and at the most basic level it is a machine that can produce beams of radioactive nuclei, or with the usual abbreviation Radioactive Ion Beams, RIB [14]. The driving mechanism in the production of these radioactive nuclei is a GeV proton source, currently the PS-Booster. Figure 2.1 shows the placement of ISOLDE in the integrated CERN accelerator structure.

The ISOL-method for production differs from the second popular method for producing RIB's, In-Flight, in that the produced nuclei are stopped, extracted and then separated, while In-Flight uses the momentum of the produced nuclei to separate directly after production. For this reason In-Flight facilities operate at much higher beam energies then ISOLDE [15].

The current ISOLDE began operation in 1992 after the entire facility was physically moved to receive proton beams from the PS-booster [16]. It

---

[1]Some, notably Danish, voices claim that the "DE" is an acronym for Danish Engineering, but while it is true that Danish physicists played a major role in the creation of ISOLDE, it is doubtful the collaboration would name a facility after one single country
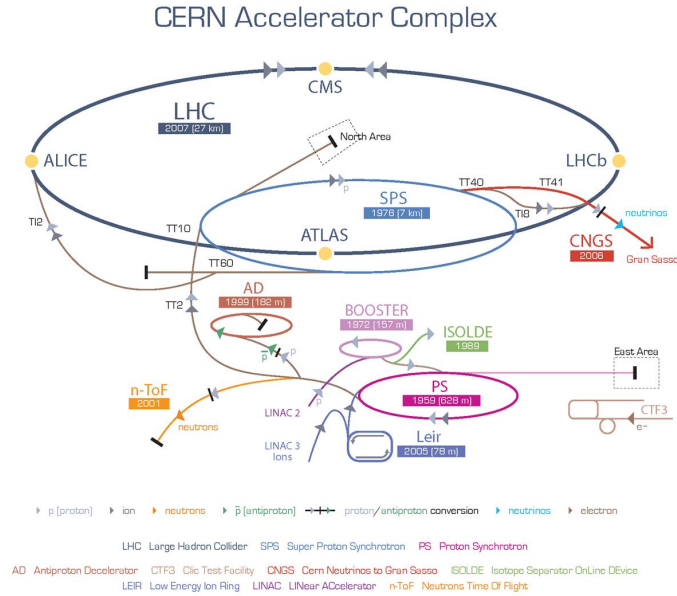
Figure 2.1: The CERN accelerator structure. ISOLDE is in green on the right. The picture is from the CERN web site

is the successor to one of the earliest on-line isotope separators ever built. The work on the first ISOLDE started as early 1964 with the approval of the project by then CERN director V.F Weisskopf. Since then ISOLDE has evolved from a minor experiment to a major CERN facility with over 300 users from 80 institutions in 21 countries. A wide range of physics experiments is now conducted at ISOLDE within many fields [17].

In the following sections I will attempt to give an overview of the current facility layout, its components and their interactions, by following the beam through the facility from production to the experimental setup. In section 2.2 we will take a closer look at the REX-ISOLDE post-accelerator where the experiment presented in the later chapters has been performed. In figure 2.2 a map of ISOLDE and REX can be seen, the highlighted line shows the path of the beam used in our experiment.

As mentioned before the driver behind ISOLDE is the accelerator called PS-booster. This booster deliveres protons to a range of facilities at CERN, including eventually the LHC, seefigure 2.1, and so does not exclusively supply ISOLDE. Every 1.2 seconds PS-booster ejects a bunch of up to $3 \cdot 10^{13}$ protons with an energy of 1.4 GeV and a pulse length of 2.4μs . The protons are delivered in what is called a super cycle of 12 bunches that repeats every
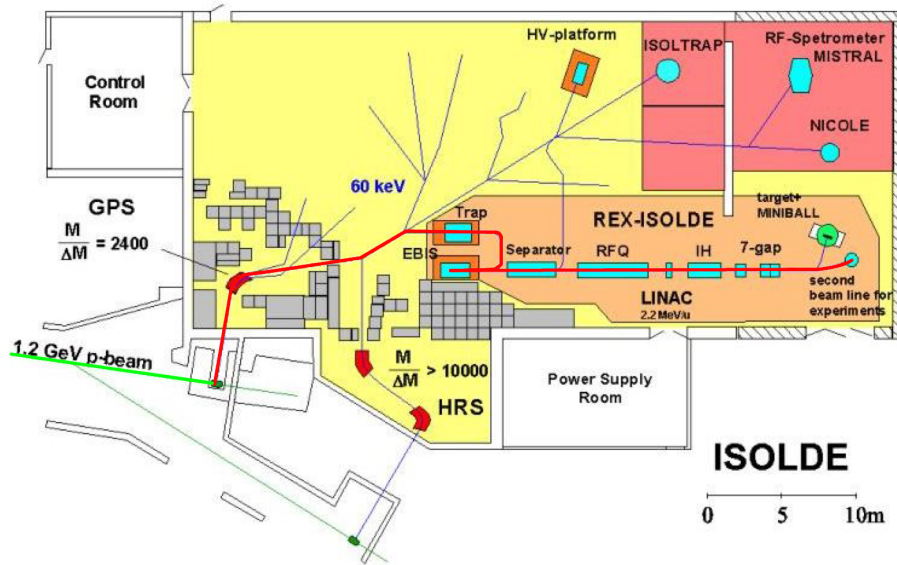
15

Figure 2.2: Map of ISOLDE. Proton beam is green, ion beam red. Note this map is outdated since it does not include the 3 MeV REX upgrade, that we will return to in section 2.2.

14.4 seconds [2], since this is a shared resource on average little more then half of these bunches go to ISOLDE. [16]

2.1.1 Primary target

The production of radioactive nuclei happens when the proton beam impinges on the primary target. This target can be made of a range of differing materials, usually containing a heavy element like Lead or Uranium, and can be either a solid or a liquid. A huge effort has been put into target development at ISOLDE making it a world leader in the production of many elements and isotopes. (cite?)

The actual production mechanism depends on target type and specific nucleus. The mechanisms are graphically presented in figure 2.1.1. The first mechanism is spallation, where a number of individual nucleons are removed from the heavy nucleus producing a rather heavy fragment for further study. The second is fragmentation where a small fragment nucleus, in the illustration ^{11}Li, is produced along with a heavy fragment and individual nucleons. For studying light nuclei far from stability you want to maximize this mechanism. The third method is fission which gives two medium sized

---

[2]The structure of the super cycle has been up for review in preparation for the start of LHC and so has the energy of the protons. However, during this experiment the old super cycle structure was still used
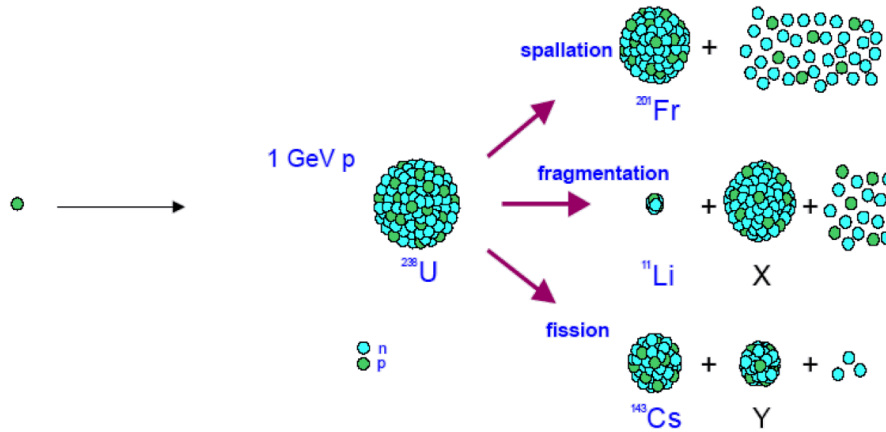
Figure 2.3: The different ISOL production mechanisms.

nuclei and some individual neutrons. The last method can be enhanced by using a neutron converter where the proton beam impinges on this instead of directly on the target, thus showering the target with neutrons instead. Optimizing different target types for different isotopes is a science in and of itself, see e.g. [18] and we shall not be concerned with this any further in this thesis.

In order for the produced nuclei to be useful they need to be extracted from within the target material. This is done through diffusion. An electrical current heats the target to several thousands of Kelvin and the produced nuclei diffuse out of the target material and into the ion-source via a transfer line. The avarage time-scale for this diffusion process is around 100 milliseconds, but since some nucleons will diffuse much faster than this, it is possible to work with elements that have half lives down to about 5 ms. A graphical illustration of this process can be seen on figure 2.1.1

ISOLDE has two primary target stations, each with its own separator magnet from which they get their name; the General Purpose Separator, or GPS target station and the High Resolution Separator, or HRS target station. As can be seen on figure 2.2 we used the GPS in our experiment. We return briefly to the separators in section 2.1.3.

2.1.2 Ion source

When a nucleus exits the target material it is in the form of a neutral atom. In order to accelerate the nucleus, and its electrons, it needs to be ionized.
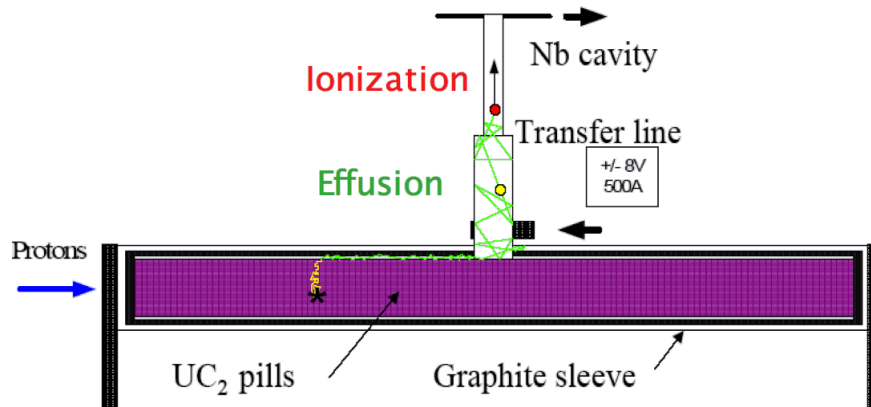
17

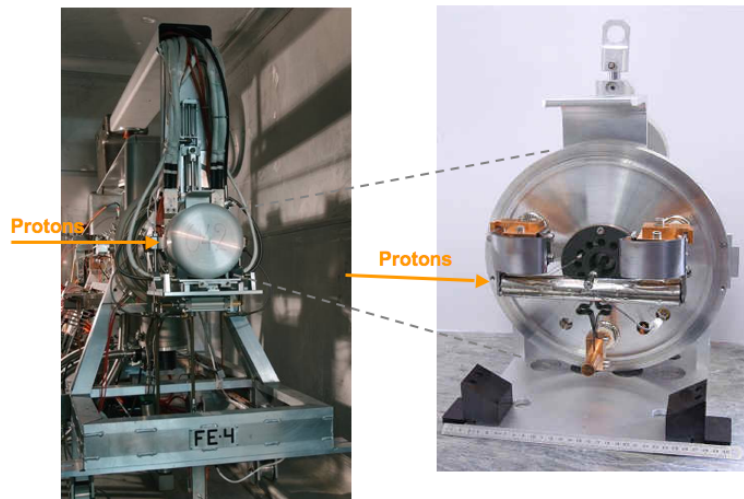Figure 2.4: The created nucleus diffuses out of the target material and ends up in the ion source.

Figure 2.5: Left picture shows the whole front end and on the right is a picture of a single target unit. The tube in the middle is the target holder. The Copper heating electrodes used to heat the target holder can be seen on either side of the tube.
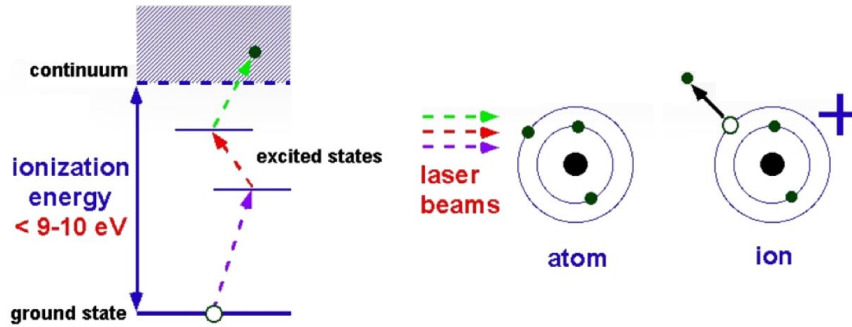
Figure 2.6: An illustration of the principle behind RILIS.

The ion source is mounted very close to the target holder in a single target unit, seen on figure 2.1.2. The target holder is the cylindrical, horizontal tube, and the ion source is the unit seen behind the small transportation line from the target. When mounted, the unit is shielded by an aluminum shield somewhat resembling, and thus named, a cooking pot.

As part of the effort to increase the number of beams available at ISOLDE, a range of ion-sources has been developed. At the moment surface ionisation, plasma ionization, and laser ionization sources are available, the newest and most advanced being the laser ion source RILIS. The choice of ion source depends on the characteristics of the element studied as well as possible contaminants in a beam containing such an element. Surface ionization does not work for nuclei that stick to surfaces, and since a wide range of nuclei is produced in the target a non-selective ionization method might contaminate the beam beyond what can be cleaned up in the separators. For our experiment we used the RILIS ion source which we will now discuss

RILIS

RILIS is shorthand for Resonant Ionization Laser Ion Source [19]. It uses a set of two or three superposed laser beams in order to perform a stepwise and highly selective ionization. The laser beams are sent through a window of quartz and directly into the ion source. By choosing the wavelengths of the photons to match transitions to either an auto-ionizing state or the continuum RILIS allows for the ionization of a specific element, and for nuclei with a very large hyperfine splitting even a specific isomer [20], see figure 2.1.2.

Since the RILIS lasers are pumped lasers, operating at a repetition rate of around 10kHz, the ionized beam attains a time structure that can be used to gate events in an experiment. As we will see later though, the REX linac
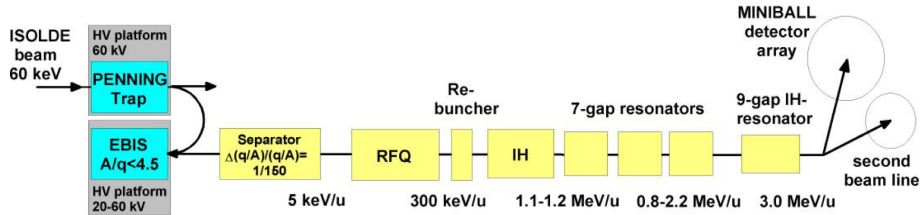
19

Figure 2.7: Schematic overview of REX .

removes this time structure and replaces it with another one. As a side-note it is worth mentioning that the time structure from RILIS was used for something else in our experiment, namely as a veto in the data acquisition since the electromagnetic burst from the lasers firing triggered our setup.

2.1.3   Isotope separation

From the ion-source the now charged nuclei passes through a potential drop of between 30 and 60kV and some focusing quadropoles to give us a beam of 30-60keV ions. Depending on the target station the beam then passes through either the GPS or the HRS, both of them magnetic separators that perform a mass over charge or A/Q separation. Making the reasonable assumption that all ions are singly charged, so $Q = 1$, this gives us a mass selection. With the element selection performed by RILIS we now, in theory, have a beam of a single isotope.

After separation, the beam can be steered to one of the many permanent experiments on the low energy beam lines or to a temporary setup in what is called the LA1 area e.g. for decay experiments. A different option is to direct the beam to the REX-ISOLDE post accelerator structure which can currently accelerate the beam up to 3.0 MeV/u. This is what was done in our experiment, so below we will elaborate a bit on REX.

2.2   REX-ISOLDE

REX was one of the first post accelerators to be added to an ISOL facility. As mentioned, it currently allows for the produced unstable nuclei to be accelerated up to 3.0 MeV/u [22]. Since its first experiment in 2002 it has contributed to knowledge in nuclear physics and several other fields by allowing a new type of experiment with low energy unstable nuclei. The first nuclear reaction experiment at REX was done by our collaboration in 2002 and was ^{9}Li+d [21]. The experiment in this thesis with beryllium follows as a direct continuation of the lithium experiment of 2002.

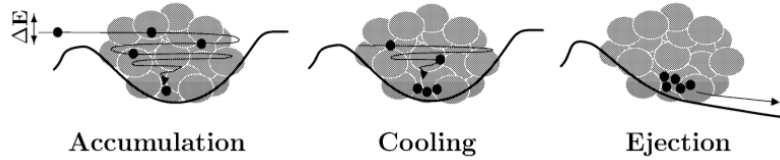The layout of REX can be seen schematically in figure 2.7. The path the

Figure 2.8: Schematic view of the cooling process of REX-Trap. The incoming potential barrier is just high enough to let ions from the ISOLDE beam enter the trap. After injection, interaction with the buffer-gas cools the ions, and they are trapped. Finally the potential barrier is lowered on the opposite side and the ions exit the trap. Figure from [23].

beam takes from injection into REX and until it reaches the experimental setup can be broken into four steps; trapping and cooling, charge breeding, separation, and acceleration. We will elaborate on each of these below.

2.2.1 REX-trap

The first element in the REX structure is a penning trap aptly named REX-Trap. It serves several purposes related to acceleration and beam properties. Trapping and bunching the semi-continuous ISOLDE beam increases the efficiency of the subsequent injection into the next step, the EBIS, which we shall return to below. Bunching also allows for a higher signal-to-noise level in experiments. This can be crucial when working with short lived isotopes in a radioactive beam. And finally the cooling of the ions reduces the beam emittance allowing for more efficient acceleration in the linac [23].

The trap is placed on a high voltage platform at up to 60kV, corresponding to the beam energy, and cools by letting the ions interact with a cold buffer-gas. The properties of this buffer-gas, and the contaminants in it, is not a trivial matter. Since mass-separation in magnets is done through selection of A/Q-values, any buffer gas element with an A/Q similar to the isotope we are interested in will be treated the same from this point on and end up at our setup. Chemically the buffer gas needs to be an inert element, for obvious reasons, and is usually either Neon, Argon or Helium.

Since natural Neon contains 9.25% of the isotope ^{22}Ne selecting ^{11}Be^{4+} would possibly give us a ^{22}Ne^{8+} contaminant in our beam. For that reason, in our experiment we used a purified 99.9% ^{20}Ne as buffer gas in REX-Trap. Aside from the actual buffer gas, atmospheric gases will also be present in the trap at non-negligible levels. Mainly Carbon, Nitrogen and Oxygen, but isotopes of these do not interfere with our experiment.

2.2.2 EBIS

After bunching and cooling in REX-Trap, the ions are moved via a transfer line to REX-EBIS. The EBIS is an Electron Beam Ion Source capable of charge breeding ions to a very high charge state [24]. The high charge eases the subsequent acceleration of the ions significantly and it is the ability to ionize to highly charged state that enables REX to accelerate heavy ions at current efficiencies.

The ion source works using a highly focused mono-energetic electron beam from an electron gun. This beam radially confines the ions while the end confinement is done by electrodes. The ions are charge bred by collision with the electron beam until they are extracted by lowering one of the endpoint potentials, similarly to what was seen for REX-trap in the figure 2.8.

The EBIS introduces another possible complication when working with certain light nuclei. During use carbon-isotopes from the residual gas are ionized along with the intended nudlei and if some of these match the used A/Q value a nasty contaminant is added to the beam. This is very clear when working with $^{12}Be^{4+}$ where $^{12}C^{4+}$ contaminates. In this case though the problem can be somewhat rectified by inserting stripper foils in the linac as we shall see below. The EBIS also adds a range of other ions to the beam from other residual gasses present in the source. This include Sodium, Potassium and Calcium, and is part of the reason for the separator we shall return to below.

The EBIS contributes one more crucial aspect to the setup. Since both REX-trap and EBIS works with bunches of nuclei, they add a time structure to the beam they deliver. The EBIS usually has a repetition rate of 50Hz, while the typical bunch length is a few hundred micro seconds. This leaves a lot of time between interesting particles reaching the setup. By adding the EBIS-time to the acquisition system and data-structure it is possible, off-line, to gate on events in EBIS-bunches. In this way some background contributions can be easily estimated.

While this bunching in many ways is an advantage, it also creates some challenges. With the very short bunch-length, dead-time becomes very important since the difference in statistics between being able to measure one,two, or three events per bunch is quite dramatic. We will return to this point in the section 3.4.

2.2.3 Separation and acceleration structure

Since the intensity of the radioactive ions out of the EBIS is much lower than that of the residual ions, by up to a factor of 100, a mass separator is needed after the extraction of the beam from EBIS [25]. This separator has an A/Q resolution of ≈ 150 and is thus not a very precise instrument. It is, however,

sufficient to remove the heavier residual elements when working with light nuclei. Since the EBIS is physically located over 3 meters above the REX beam-line on top of REX-Trap, this separator also serves as a transfer line to the accelerator.

The accelerator structure itself has a number of elements. The original design had a "front part" [26] consisting of an RFQ, a re-buncher, and an IH structure, and a second part consisting of three 7-gap resonators [27]. The maximum energy with this setup was 2.2MeV/u. Since then a further 9-gap resonator has been added to the beam-line and the maximum energy, when everything is running, is now 3.0MeV/u. For our experiment everything was not running, and so our beam energy was limited to 2.25MeV/u.

As mentioned before, contamination by Carbon isotopes from the EBIS electron gun can be a huge problem. This can be somewhat remedied for nuclei with $Z < 6$ by using the highest charge state available of the isotope under investigation and then inserting stripper foils in the accelerator structure. This will strip electrons of the Carbon ion, leaving the ion under investigation untouched and only marginally increase beam emmitance through straggling. Stripping will put the Carbon ions out of phase with the acceleration structure, optimized for a certain A/Q, and also allow for a degree of separation in the final bending magnet. This technique can also be used for other A/Q contaminants, and in our experiment several stripping foils were inserted to get rid of an initial remnant of ^{22}Ne from the old REX-trap buffer gas. This remnant however disappeared after one day of running by itself.

2.2.4   Beam and time structure

We are now able to go back to figure 2.2 and understand the production of our beam of ^{11}Be as well as the time structure of it when it reaches our setup. The radioactive nuclei are produced by bombardment of a solid state tantalum target by 1.4 GeV protons. The produced nuclei diffuse out of the target holder and into the ion-source where a very selective laser ionization takes place. As ions, the nuclei are extracted from the ion-source and separated in the GPS before being injected into REX-trap. Here the ions are bunched and cooled before being injected into REX-EBIS to be charge bred. With no electrons left, the nuclei are again ejected at 50Hz and in 200μs bunches through the REX-separator and into the linac, which gives them a kinetic energy of 2.25 MeV/u. The efficiency of the process through REX is, depending on half lives and mass, 5%-15%, lowest for the lightest nuclei.

Chapter 3

Experimental Setup and Analysis Techniques

In this chapter we will cover the equipment and setup used in our specific experiment, as well as the techniques used for treating and analyzing the data obtained. We will start with the hardware closest to the reaction and move outwards ending in our acquisition system and our software.

3.1 Setup

The detector setup can be seen schematically in figure 3.1. The beam from REX enters our setup from the left through a 4mm tungsten collimator. Behind this collimator is our target ladder which holds all of our solid state target foils. The ladder holds four foils at a time exposing a circle with a diameter of around 1.2cm each to the beam, one at a time. For this experiment the ladder held two foils of deuterated polyethylene with thicknesses of $16.9\pm0.2\mu$m and $7.5\pm0.5\mu$m respectively, one regular polyethylene (PE)
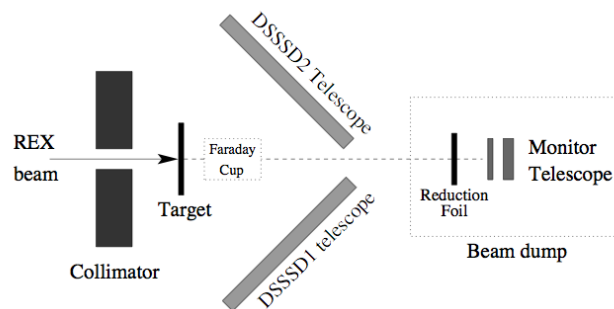
Figure 3.1: Our setup
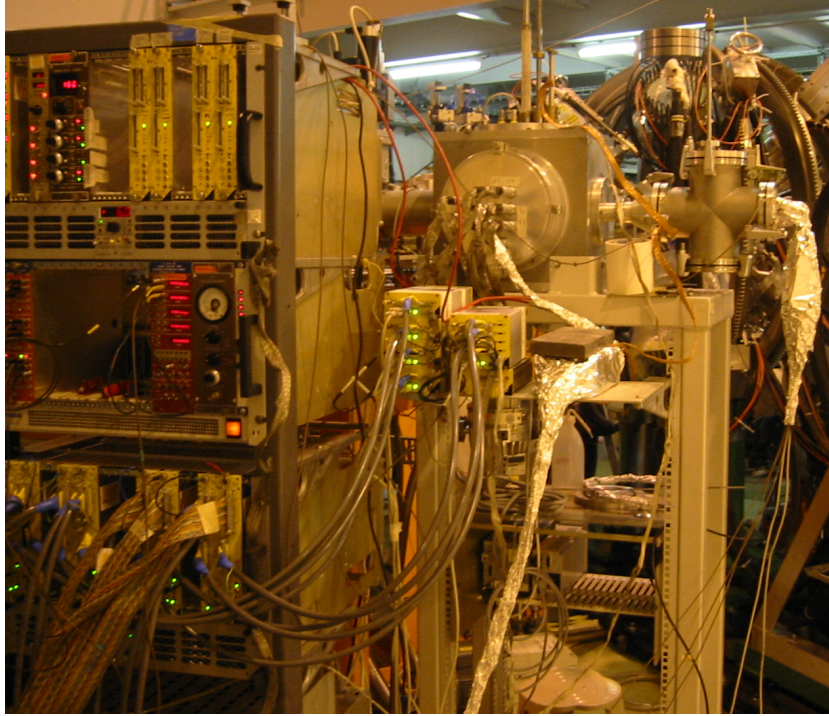
Figure 3.2: A picture of the setup seen from the outside

foil with a thickness of $15\pm1\mu$m,. and finally a Silver target for Rutherford scattering with a thickness of $1.04\pm0.05\mu$m.

Behind the target ladder was placed a Faraday cup used for tuning the REX linac with stable beam. This cup was on a stick so we were able to take it out of the way when it was not needed. Behind all this we had two Double Sided Silicon Strip Detectors in telescope with a thick Si-Pad detector, both placed at backwards angles in relation to the target and beam. We will take a closer look at the DSSSDs in the next section.

All of the above was housed in our target chamber, seen from the outside on the right in figure 3.2. This is an aluminum box of approximately 34cm by 34cm by 24cm. The size of the chamber poses quite a challenge when cabling for over 130 data channels as in this experiment, but makes for a rather easy volume to pump.

The final part of our setup was mounted behind the chamber in a sort of beam dump, it can be seen as the cross mounted behind the chamber in figure 3.2 and also in figure 3.1. Since most of the beam passes straight through the target without interacting, the beam dump contains several reduction foils in order not to sputter the detectors or overload the DAQ

Figure 3.3: A computer generated image of one of our old 16 strip DSSSDs. Unfortunately we do not have any pictures of our new model with 32 strips.

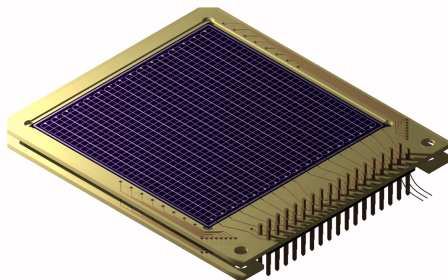system.[1] Behind these foils two small non-segmented silicon detectors with thicknesses of 10μm and 700μm were mounted in telescope. The beam dump detectors allowed for online monitoring of both relative beam intensity as well as purity. However, we were not able to calibrate the transmission from the target ladder to the monitor telescope, and so we are unable to extract absolute beam intensities from this.

3.2 Detectors

The cornerstone detectors used in our experiment were, as mentioned earlier, Double Sided Silicon Strip Detectors or DSSSDs. These thin silicon wafers, approximately 60μm in thickness and 6.4cm by 6.4 cm, are segmented into 32 strips on each side. The two sets of strips are perpendicular to each other and back and front strips thus divides the detector into 1024 pixels. A computer generated image of a detector can be seen in figure 3.3.

The detectors are run with reverse bias to deplete and enlarge the active region in the detector, the part doing the actual detection, as well as increase the efficiency of charge collection. We shall return to the generation and detection of signals in silicon detectors in Chapter 6.

This type of detector has played a central role in the work of our group and collaboration for the last 6-7 years. Since the first models were used [29], a number of improvements has been made to them by our collaboration. A new set of detectors with a very thin inactive or dead layer on the front side [30] has been designed. The term dead-layer comes from the fact that energy lost here is not seen in the data. Another innovative design has been an increase in the number of strips. As stated above our newest detectors have 32×32 strips an increase from the 16×16 on the first versions. The new

---

[1]Although we are getting ahead of ourselves here, the beam dump was eventually taken out of the triggering mechanism to minimize dead-time

version also has a non-reinforced edge, enabling the detector to be placed very close to the beam, but unfortunately also making it very fragile.[2]

Each DSSSD is backed by a thick 1500μm Si-pad detector in order to stop the charged particles completely. In this way we measure the total energy of all charged particles. The setup of DSSSD and Si-pad also allows us to identify individual particles with charge one or two and sufficient energy, e.g. protons or deuterons as we will see in section 3.6. The Si-pad detector functions more or less as a single DSSSD channel in regards to readout and calibration, and we shall not treat it in any further detail in the following.

3.3 The electronics chain

The signal generated by the DSSSDs and the back detectors goes through a range of different electronic devices before information about it is stored on hard-drive by the acquisition system. Understanding this electronics chain and the Data Acquisition system, or DAQ, itself can initially seem like a daunting task[3], but is actually not that difficult. This knowledge is important for a number of reasons. First of all, during setup of an experiment it enables troubleshooting of common problems like broken cables and modules or bad analysis software, all important things to get remedied before an experiment starts. Secondly, in the unfortunate event that something was not working under the actual experiment, finding the malfunction off-line also requires knowledge of the electronics and the DAQ. At this stage, since the setup is torn apart, you have to rely on documentation from the logbook, so this is also crucial. Detailed knowledge of the workings of all of the electronics also turns out to be extremely important in order to study the signals generated directly by the detector. This is exactly what we propose to do in DLEP, as we shall see in chapter 6. For those reason we spend some time on the subject here.

3.3.1 Modules

A schematic drawing of the electronics chain can be seen in figure 3.4. Below we will look at the function of each of the modules in this chain.

The signal is initially generated by a charged particle impinging on the DSSSD. As we shall see in chapter 6 this creates a signal of a few millivolts with a rise time of around 10 ns. In order to transport this signal over anything but very short distances it needs to be amplified. For this reason the first step in the chain, Pre Amplification, is as close as possible to the chamber. Also, since the signal is so small at this stage, keeping noise out is very important.

---

[2]So far three of four 32×32 DSSSD have been destroyed during handling...

[3]A small idea of the amount of cabling involved in an average experiment can be seen in figure 3.2, showing chamber with preamps next to it and shapers in the foreground.
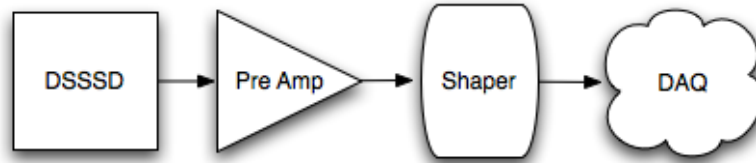
Figure 3.4: A schematic drawing of the electronics chain. The signal generated by the DSSSD passes through a pre amplifier and shaper before being converted to digital in the ADC and stored by the DAQ.

Pre Amplifier

The pre amplifiers used in our experiment were of the Mesytec MPR 16 and 64 channel type, specifically designed with DSSSDs in mind. The preamp is a very dumb charge amplifier, taking any and all signals that it gets as input and simply amplifying them by a specific factor, or a specific gain. Depending on the type of preamp, this happens at a particular time-scale that is given by the time from which the preamp has collected a certain amount of charge and until the amplified signal reflects exactly this charge. For our preamps this time-scale is 10 ns, and thus of the same order of magnitude as the signal in the DSSSDs. This is sufficient for our applications in this experiment.

While the preamp signal is relatively fast in the way up, it falls off rather slowly. A typical fall-time is 50-80μs and thus 3-4 orders of magnitude larger than the rise-time (see the top signal in figure 3.5). This could potentially be critical in case another particle enters the same channel before the preamp has reset. This would generate a signal representing a larger energy than the particle physically had. For this and other reasons the next step in the chain is a shaping module.

Shaper

The shaping module serves several purposes besides removing the possible problem of pile-up from the preamp signal. The longevity of the preamp signal could also be a problem for dead-time. This is defined as the amount of time new particles hitting the detector are not recorded after it has been hit by an initial particle. For this reason the shaper cuts the tail away from the preamp signal. This can be done because all the information about the particle is in the height of the signal, proportional to the amount of charge generated in the DSSSD, and not in the tail.

From the leading edge of the pre-amp signal a fast signal is generated, with no energy information to be used for timing purposes. This allows one,
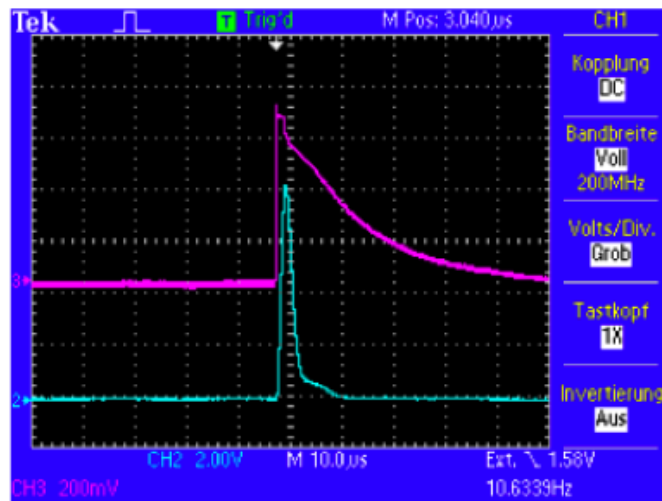
Figure 3.5: An illustration of the difference between a preamp signal, above in red, and the corresponding shaper signal, below in blue. One unit on the x-axis corresponds to 10 μs, y-axis is 200mV and 2.00V respectively. The illustration is from Mesytec

in theory at least, to discriminate between the timing of individual particles within a single event. The timing signals were not and have not been used in this experiment, even though they were at least partially set up, so we shall not comment on them any further.

One further signal that is generated by the shaper the trigger signal. This is the signal that tells the acquisition that something interesting is going on and that it should start recording. The threshold for the trigger, the minimum height a signal must have before triggering, is thus also set in this module. We will take a further look at the trigger and trigger signals in the next section.

Finally the shaper also amplifies the energy signal to the desired voltage for use in the digitization process. Since the next module, the Amplitude to Digital Converter or ADC, has a fixed range of conversion, the energy range of the experiment is fixed by the combined amplification of preamp and shaper.

The shapers used in our experiment were also from Mesytec, and of type STM 16+. In figure 3.5 an illustration of the difference between a shaper signal and the preamp signal can be seen.

Amplitude to Digital Converter, ADC

The shaper passes the signal on to the Amplitude to Digital converter, or ADC. The main feature of this module is that it converts the height of the voltage signal to a digital value. Our ADCs were CAEN V785 Peak Sensing ones with a range of 8V and 4096 channels. This means that a signal peak between 0V and 8V would be converted to a numerical value between 0 and 4095 linearly. Each module has 32 channels, and thus contains only enough for one side of our DSSSDs.

As mentioned earlier the ADC is told when to look for an incoming signal via the trigger from the shaper. Usually a module can only hold one value for each channel and thus has to be read out or at least reset after each event. Event in this context means that a trigger signal has been received by the ADC, and thus that it has *looked* for a signal that may or may not be there.[4] In the case that no signal was incoming, all channels will hold the value 0 but they will still be full. The last feature of the ADCs that we shall mention here is that this particular model has an event-buffer. This means that it can store up to 32 events before needing to be read out. The importance of this we shall see in the next section but first, for completeness, we will look at one final module, a scaler.

Scalers

Scalers are very simple and very useful modules that are basically counters. What a particular channel in a scalar counts can be anything; triggers, EBIS-pulses, Proton-pulses. As long as it generates an electric signal it can be counted. Scalars can be either analog, meaning that they simply output values on a display or digital meaning they can be read out in the same way as the ADCs. Since we have said nothing about how this is done we now move on to the next section where this is covered.

3.4   The DAQ

During the summer of 2005 I spent three weeks at CERN together with Haakan Johansson setting up and running the DAQ used for our experiment. Since we[5] ended up experimenting quite a lot with the setup and running of the DAQ I will spend considerable effort explaining what was done and why. For the more technically inclined I recommend Haakans thesis The Data Acquisition system, or DAQ, is the common name for the unit or system that collects and records all signals, physics and otherwise, from the experiment. For the energy data it is responsible for converting output from the shapers to bits on a hard-drive, while keeping information about the

---

[4]Not e.g. if the trigger was generated by noise from lets say a laser firing
[5]In the loosest possible definition of we. I watched and learned from the master

circumstances under which the event took place, which detector and which strips were hit, how long after proton impact, and so on.

Since the DAQ handles the recording of all physics information, or actually all information coming in electronic form, the operation of the DAQ is critical. A malfunctioning or unstable DAQ can ruin an experiment.

Together with all the conversion modules the DAQ has three other major components; a processing unit with network access[6], a trigger module, and one or several crates where everything is placed. The electronics built into the crate, called a VME Bus, can be compared to the workings of a regular PC motherboard. The processing unit accesses the different modules through the bus. The crate also supplies power.

The processing unit used for this experiment was running the GSI-developed Multi Branch System, MBS, acquisition program on top of a Lynx operating system.

The trigger module is a separate module that collects all triggers and informs the processing unit that they have occurred. The reason for this module is that usually you allow triggers for other events than just a particle hitting the detector, and with this module you can identify which events are from which trigger. The trigger module also has a "busy" output. This is used to broadcast a "System Busy"-signal while the processor is running, or during read-out of the modules.

The data collected by the DAQ was uploaded via the CERN network to a storage computer which allowed us to access the data nearly online. A final feature of the DAQ was the broadcasting of the scaler values over the network, allowing any computer accessing the network to, in principle, read out the real time scaler values.[7]

3.4.1 Dead-time and trigger logic

As mentioned earlier dead-time is the time when a particle hitting our detectors would not be recorded by the DAQ. We have already touched on some of the contributions to dead-time and we will elaborate a bit below. It should be clear that this time needs to be minimized. Working with a pulsed and bunched beam of particles as we do with our beam from EBIS makes this even more important.

It can be fruitful to think of dead-time as recovery time: The time it takes for the detection system to recover after being hit by a particle. The preamp for instance takes 15μs to recover after having amplified a signal. Any particle hitting within these 15μs would be assigned a wrong energy value. Since nothing is prohibiting this signal being passed down the electronics chain, it would be recorded by the DAQ with the wrong energy. This kind

---

[6]Most people would call this a computer, but its a highly specialized one.

[7]Practical for optimizing the REX-linac, but also to see if everything is running okay while having lunch.
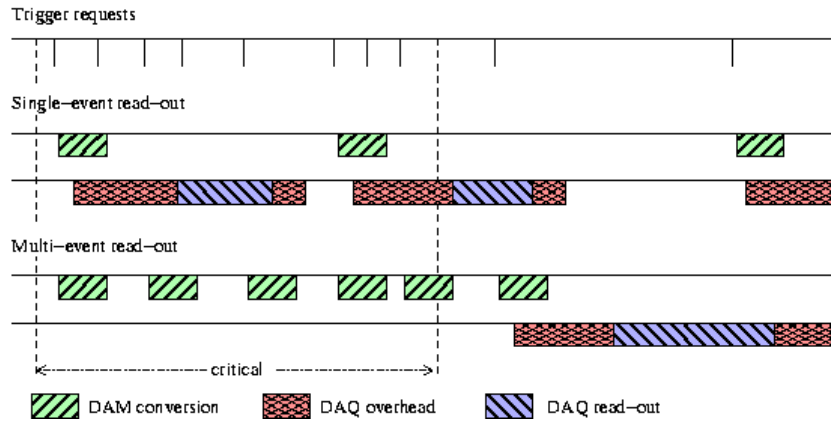
Figure 3.6: The same set of triggers (top panel) leads to significantly different amounts of recorded data for a DAQ running in single- or multi-event mode. Figure adapted from H. Johansson [32]

of dead-time is called soft dead-time because on the surface nothing tells you if your setup is in soft dead-time.

The other type of dead-time is hard dead-time when the DAQ accepts no triggers. In laboratory slang the triggers are "Vetoed". This happens for instance during read-out of the ADCs when the trigger module is broadcasting "busy". It is very beneficial, if possible, to convert any soft dead-time to hard dead-time.

There might be other than internal reason for not accepting any triggers. As mentioned earlier, in our case the electromagnetic radiation-burst from the RILIS lasers triggered our setup. This can be handled by forcing the setup to not accept any triggers while RILIS is firing, or as we shall see in a moment, by adding the RILIS firing signal to our veto.

With all this we now come to specifics.

Single event

The trigger setup, that is the way incoming triggers are handled by the DAQ, has usually been in what can be called single event mode. This means that every time a trigger is accepted(passes the veto) we convert the incoming data in our ADCs, read out all modules and send the packaged data through the network. A single event causes a full read-out of everything.

To avoid any soft dead-time we add a fast signal to the veto as soon as a trigger is accepted, thus avoiding the lag before the trigger module starts broadcasting. This means that we are in dead-time from when the trigger is accepted and until the data is transferred over the network to storage. Figure 3.6 illustrates how the time is being used for a particular set

of triggers. DAM is Data Modules (ADCs and Scalers) which use around $20\mu s$ to convert the incoming data to digital. The total dead-time in our setup was measured to be between 100 and $150\mu s$ including the read-out of modules and broadcasting over the network. Now since the EBIS-pulse is only around $200\mu s$ long (the "Critical" period in figure 3.6) this means that at best we can accept two events per pulse running in single event mode.

Multi event

In order to make the number of possible accepted events per EBIS pulse larger, we need to bring down the dead-time. It is clear from figure 3.6 that the main contributor to dead-time is the read-out and associated overhead performed by the processing unit. If we could wait with the read-out until after the EBIS-pulse then we would only have the dead-time associated with the data modules converting. Waiting with the readout is only possible if the ADCs and scalers can store several data values for a period of time. As mentioned earlier this was exactly the case for the ones we used, and led to the development of the multi event triggering scheme for this experiment.

In single event mode all triggers are equal and lead to a full readout of all modules. In the new multi-event mode physics triggers are treated as a special case. If we look at figure 3.7 all other triggers still go to the trigger module and lead to a full readout, but physics triggers only start conversion in the modules. Now in order to keep track of dead-time the modules themselves must broadcast a busy-signal while converting and this is then added as dead-time. Since this conversion time is much shorter than a full read-out, only $20~\mu s$, we are able to handle many more events than in single event mode (see figure 3.6).

The final detail of this scheme is to ensure that the event buffer never gets full, we need to read out some times. Since REX-EBIS runs at 50Hz there is plenty of time between pulses to perform a readout. The solution we choose was to delay the EBIS release-signal in order to put it well after the bunch, and then use that as read-out trigger. This had the fortunate side-effect of putting a running clock in our data-stream since all EBIS-pulses was counted in this way. As an extra precaution each individual module was programmed to force a readout in case the event buffer was filled.

3.5   Calibration

In order to use the data collected by the DAQ for any useful physics we need to calibrate the system such that each of the 4096 channels in an ADC-event can be assigned a corresponding energy value. Calibration of a DSSSD is a multi step process. Originally it was published for the 16-strip version [29], but nothing fundamental has changed since then. We will draw up the main steps in the following.
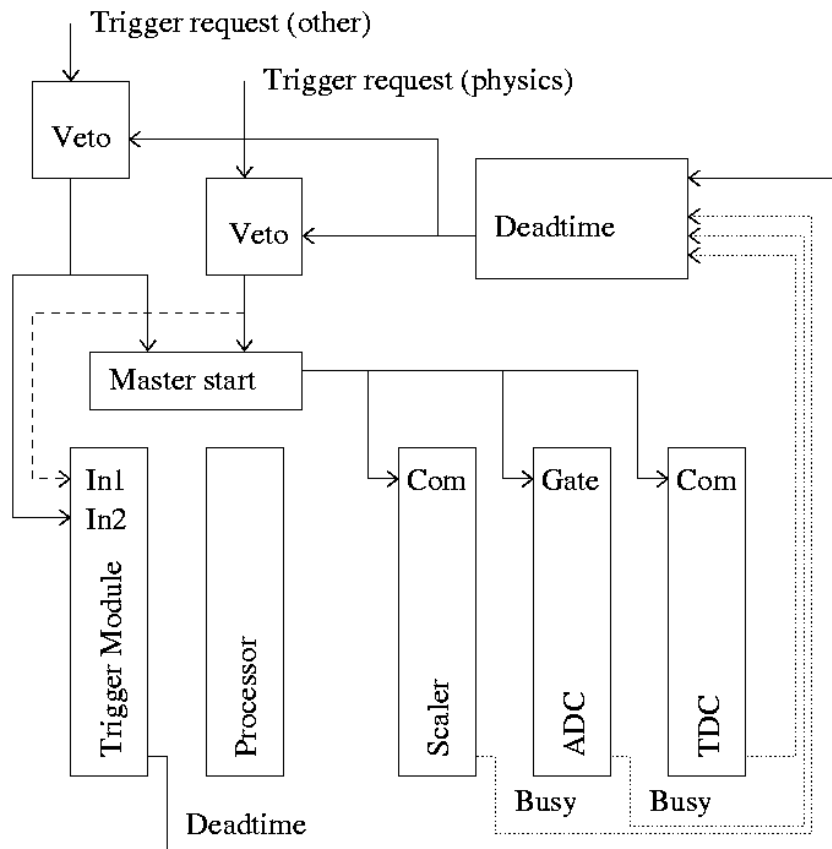
Figure 3.7: Schematic drawing of the trigger setup. In multi event mode, the dashed line is removed and the dotted lines are added to the setup (see the text for details). Figure adopted from H. Johansson [32]

Our DSSSDs were calibrated using α-sources. For certain ISOLDE experiments it can be beneficial to use online sources, but for this experiment we used only offline ones. The sources were placed on the target ladder instead of the foils and radiated each detector facing them individually. We used four different isotopes to calibrate physically placed on two different sources. The first source was a ^{148}Gd-source and the second source consisted of ^{241}Am, ^{239}Pu, and ^{244}Cm. We shall return to the particular properties of each source below.

The granularity of the detector both helps and complicates things when calibrating. Since each strip is treated as an individual detector in the datastream, a single DSSSD has 64 channels to calibrate. On the other hand the granularity gives us some spatial information that we use to gain accuracy.

3.5.1 Solid Angle Calibration

The first step of the calibration process is to find the position of the source relative to the DSSSD. Instead of measuring this we use the granularity of the DSSSD and the fact that the source emits αs uniformly. Looking at the distribution of events across the DSSSD and using four free variables, one for the distance, two for position of DSSSD relative to the source at that distance and a normalization factor, we can fit the exact position of each source. This assumes that the source is a point source, but at the typical distance of 5-7cm and with a typical source diameter of 0.5cm this is not a bad approximation. Figure 3.8 shows the fit for DSSSD 2 in this experiment. It is clear from the figure that the source was placed slightly to the left of the center of the detector.

3.5.2 Energy Calibration

The final energy calibration is made using a simple Gaussian fit to each of the α-levels seen from the sources. Since some of the sources emit αs at more then one energy, and since these are not resolved in our detectors, we simultaneously fit all 9 levels. We utilize by the fact that the relative intensities within each resolved peak is known. The table below has the data for the decays that are seen in our calibration data.

Isotope	Energy	Branching	Energy	Branching	Energy	Branching
	MeV	%	MeV	%	MeV	%
^{148}Gd	3.182	100	-	-	-	-
^{239}Pu	5.155	73.2	5.143	15.1	5.105	10.6
^{241}Am	5.485	85.2	5.443	12.8	5.388	1.4
^{244}Cm	5.804	76.4	5.763	23.6	-	-
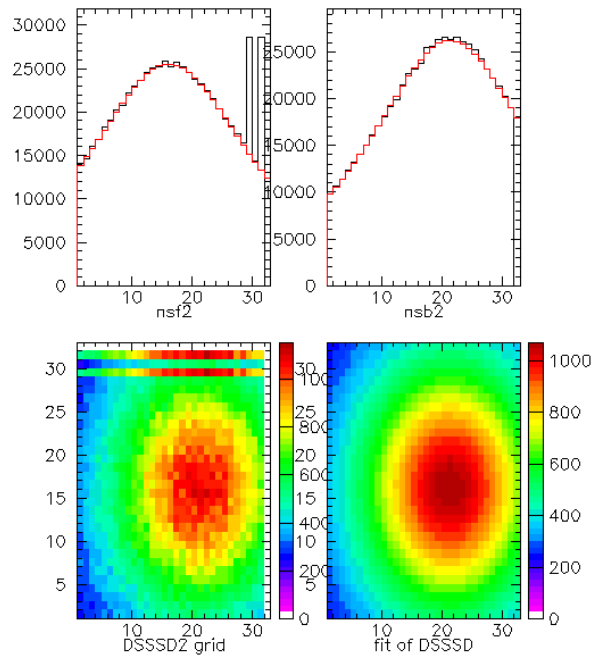
Figure 3.8: Four figures showing the solid angle fit of DSSSD2 compared to data. The two top figures show front strip (left) and back strip (right) distributions of events (black) as well as the fit (red) assuming a uniform distribution. From the figure it is clear that front strips 30 and 32 misbehave (for an unknown reason) and they were subsequently killed. In the bottom the same information is shown in 2D grid form, data on the left and simulation on the right, clearly showing the 1024 pixels.

Figure 3.9: Histogram containing all DSSSD2 triple source calibration data, the first peak fitted with a Gaussian (red).

These levels gives us four points in the (channel, energy)-space and this is enough to make a linear calibration. However, because we want maximum precision, we need to take a few effects into account before this can be done.
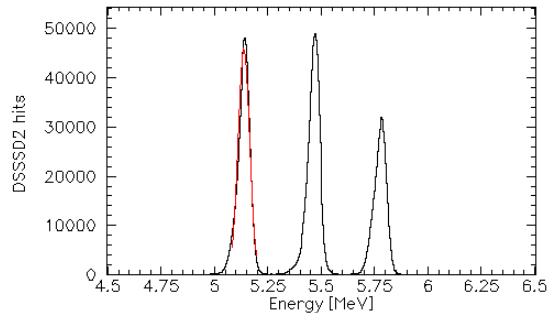
Dead-layer correction

The new 32×32 detectors have a thick dead-layer of 620nm. A particle has to pass through this before reaching the active part of the detector. This means that our alpha particles have slightly less energy when entering the active part of the detector than when they were emitted. We assume this dead-layer to be made of Si. For a 5MeV alpha particle the corresponding correction is 120 keV at right angles. At larger angles we also correct for the fact that a particle traverses even more dead-layer [29].

Some experiments chose to ignore this effect, making their calibrations effective calibrations. This can leave enough accuracy specially when working with αs in the actual experiment or when using high energies. But for our low-energy uses and in close geometry a shift of 120-200keV is significant.

Final resolution

The final resolution of our calibrated ΔE-detectors can be estimated in a rather simple manner. Using all the calibration data, in this case only from the triple source, we project a single calibrated histogram. Assuming that each peak physically should have no width, a conservative estimate since each peak has substructure as seen earlier, the resolution of our setup is simply the width of the peaks, so fitting each peak with a Gaussian gives us our resolution. In figure 3.9 the spectra obtained in this manner can be seen with one fitted Gaussian shown. This fit had $\sigma \approx 25$keV and so our resolution is around 25keV in this experiment.
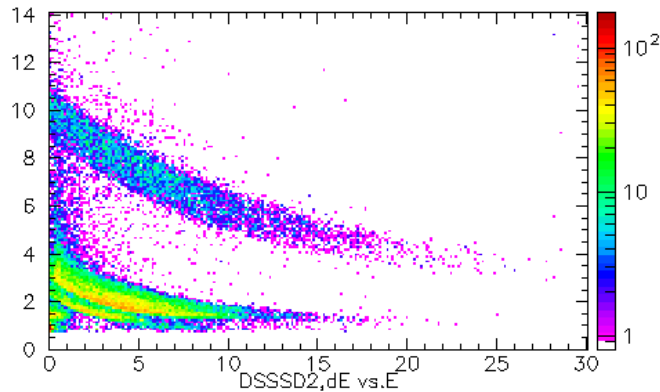
Figure 3.10: ΔE vs. E plot for data from ^{11}Be on deuterons as discussed in chapter 4. Actually the x-axis is energy, E, while the y-axis is ΔE.

3.6 Particle identification and corrections

With everything calibrated we can now take a look at some of the methods that we use in our data analysis. The first step is to identify what type of particle we see in each event. This is where our telescope setup becomes important. Simply plotting the energy that a given particle has deposited in the thick detector versus the energy deposited in the DSSSD gives us, for DSSSD2 in this data set, figure 3.10.

It is very clear that this figure has a definite structure. By looking at the stopping of particles in 60μm of Silicon, it can be seen that the wide band on top must be αs, while the bottom most structure must be charge one nuclei, this method is called $\Delta E - E$ identification and is based on the fact that nuclear stopping power is proportional to the mass and charge of an incoming particle. We shall return to this in chapter 6.

Although a lot of structure can be seen in figure 3.10, it is not easy to identify the individual charge one particles from one another. To clean up the spectrum a correction can be made to the two energies. We use the fact that particles hitting the detector at large angles pass through more of the DSSSD and thus deposit relatively more of their energy here than a particle with the same energy hitting at a right angle. The correction can be seen below in formula 3.1

$$
\begin{aligned}
\Delta E' &= \Delta E \cos\theta \\
E' &= E + (1 - \cos\theta)\Delta E.
\end{aligned}
\tag{3.1}
$$

If we use that correction on the data from figure 3.10 we get the result seen in figure 3.11. We see that the band of α particles narrow significantly
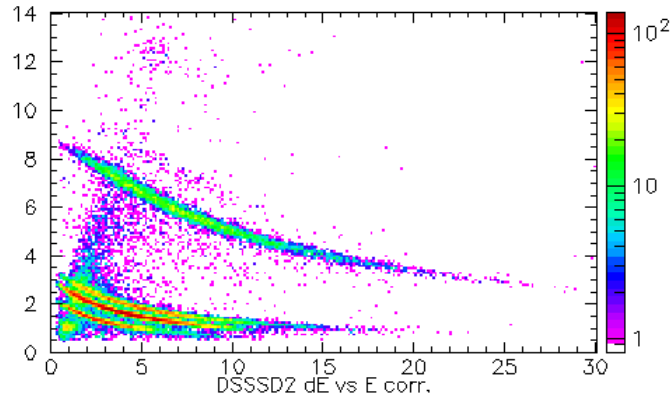
38

Figure 3.11: ΔE vs. E plot modified as discussed in section 3.6, but showing the same data as figure 3.10.

and individual charge one particles separate nicely into three bands. From this it is already clear that we see protons, deuterons and tritons in the experiment. It is important to stress that the *physical* data is the data seen in figure 3.10. The correction is only to facilitate identification of the particles.

From figure 3.10 we can see that in order to be identified with this method, a proton needs to have at least 2MeV of kinetic energy, while an α needs to have at least 8MeV. Physically any given particle must have enough energy to pass through the DSSSD and into the thick detector behind it in order to be identified. A low energy cut-off is thus a necessary evil in using the ΔE-E method. Significant resources have been put into eliminating or at least minimizing this effect. This is has led to the Detection of Low Energy Particles, or DLEP, project, financed by the European Unions sixth framework program. We return to this effort in chapter 6.

More dead-layer corrections

Having identified which particle is in a given event the appropriate corrections can now be made to the detected energy. As with the α-particles used for calibration the particles in the experiment also pass through the detector dead-layer. Furthermore they also have to escape out of the reaction foil, and lose energy there as well. Thus the resulting correction takes particle type, angle through the foil, and angle through the detector into account.

3.7 Simulations and other software

The last thing we shall turn our attention to before we move on to data is software. We use a range of software in the analysis of our data, mostly made internally and most of it written in FORTRAN using extensively the CERN programming library. Our main analysis tools are the Physics Analysis Work-tool, PAW, and the fitting suite MINUIT, both tried and tested suites of software and both originating at CERN. Our analysis software takes into account all the physics and detector effects mentioned above, but we shall not comment in any detail on specific programming.

Apart from analysis software we use simulations for a range of purposes. Firstly, simulations are used to debug and quality check the analysis software. By simulating a general set of data and knowing what physics we put in, we know what to expect when running our analysis software. This can be extremely useful for locating bugs in several thousand lines of code.

Once we are reasonably assured that our analysis software performs as expected, simulations are then used to check our physics understanding. By trying to emulate in simulation what we see in the data we can identify which part of a particular data set is well understood and which is not. This is also a great way to see if a particular feature in the data set might be caused by a real physics effect or some particular feature of our setup.

This leads us to our final application of simulation software. We use it to correct for setup specific features. More specifically we use simulations to correct for our limited angular acceptance. By simulating particles exiting our target foil in 4π in the center of mass system we can transfer to the laboratory system through simple kinematics and correct our experimental data. We shall elaborate a bit on this, and see some simulation data in chapter 4.

The simulation code is completely separate from the other analysis code, but a few of the external variables are necessarily the same and put in by hand. These include beam energy, position of the detectors, and the method for calculating energy loss. Though in the simulation it is used in reverse compared to the data analysis. The actual code, however, is separate using none of the same routines. This means that e.g. energy loss calculation bugs have difficulty to propagating from one to the other.

Chapter 4

Investigation of the ^{11}Be+d reaction

With all the technical aspects behind us we reach the real physics part of this thesis. As mentioned already, we have investigated the reaction ^{11}Be + d at REX-ISOLDE.

^{11}Be, and neighboring isotopes, have received a lot of attention the past decades and much structure information has been acquired from high energy reactions. This makes ^{11}Be the perfect place to compare structure information derived from high and low energy experiments, in particular for the transfer reaction ^{11}Be(d,t)^{10}Be. The discovery of differing B(E2) values in ^{30}Mg extracted from high and low energy demonstrates the need for such a comparison [33].

The second reason for studying this reaction is the expectation that we will be able to extract new structure information. In particular, the nucleus ^{12}Be is probed through the transfer reaction ^{11}Be(d,p)^{12}Be.

The study of reactions at REX-ISOLDE using Beryllium-isotopes is a direct continuation of the the work previously done in the collaboration using beams of ^{9}Li, see [21] and [34]. This work was the first attempt with reactions at the then new REX-facility, and it was successful in extracting structure information on the unbound nucleus ^{10}Li. The low-energy structure of ^{10}Li is needed for a complete understanding of the famous halo nucleus ^{11}Li.

The reason Beryllium-isotopes have received such a great amount of attention is that they contain an abundance of features that have been topical in the past decade.

^{11}Be has a well known one neutron halo and has been extensively studied during the past decade at beam energies from 20MeV/u and upwards. From the early break-up studies at GANIL [35] and RIKEN [36], to knockout reactions to states in ^{10}Be and ^{10}Li performed at MSU [37, 38], transfer reactions at GANIL to ^{10}Be [39], and break up reactions at 250 MeV/u at

GSI [40].

Theoretical modeling has been performed using many approaches,. Two recent examples are Coupled Discretized Continuum Channels (CDCC) descriptions of one neutron removal [41], and elastic and inelastic scattering [42]. With this much information on ^{11}Be, attention has now shifted to the neighboring isotopes that also contain some interesting features.

Another interesting features of the beryllium isotopes is the vanishing of the $N = 8$ magic number. In ^{11}Be this leads to the well know ground state inversion. The ground state of ^{11}Be is $\frac{1}{2}^{+}$ while the first excited state is $\frac{1}{2}^{-}$ with an excitation energy of 300keV. Vanishing of the $N = 8$ magic number also in ^{12}Be had been suggested already in the seventies [43] and has been supported by recent experimental data e.g. in [44].

Beryllium isotopes have also played a central role in the development of the topic of molecular-like states with a core of α-particles and neutrons in molecular like orbits. At much higher excitation energies than we have access to in this experiment, these states have been seen in ^{12}Be at excitation energies between 10-25 MeV ([45] and [46]). For information on the modeling of these structures see e.g. [47] and references therein.

Our experiment is the first time a beam of ^{11}Be, or any other halo nucleus, has been used for transfer reactions at REX-ISOLDE and also the first time ever that a low energy beam of ^{11}Be has been available for reaction studies. The purpose of this first run is to get an overview of the different reaction channels, the resolution we can achieve using only charged particle detectors, and an estimation of background contributions. It is expected that this experiment will be followed up by a second run using the lessons learned for a more dedicated study of the most interesting features.

4.1   Extraction of excitation spectra

Before we show the interesting plots from our experiment, the excitation spectra and the angular distributions, we will go through the process of how these are extracted from our data. The process is similar for all the exit channels and so we will take the ^{12}Be+p channel as a general example.

Having identified a given particle as a proton, using the method discussed in the previous chapter, and using the calibration, we know how much energy was deposited in the detector. Knowing particle type and energy, we can correct for the various dead-layer effects discussed in chapter 3, and then calculate our way back to the production energy of the proton, the energy it had right after the reaction in the target foil. Plotting these values for all protons in our data set gives us figure 4.1.

This spectrum does not have a whole lot of structure, but this is to be expected since we here show data for all angles. The next step is to use the angular resolution we gain from the granularity of our DSSSDs. Using this
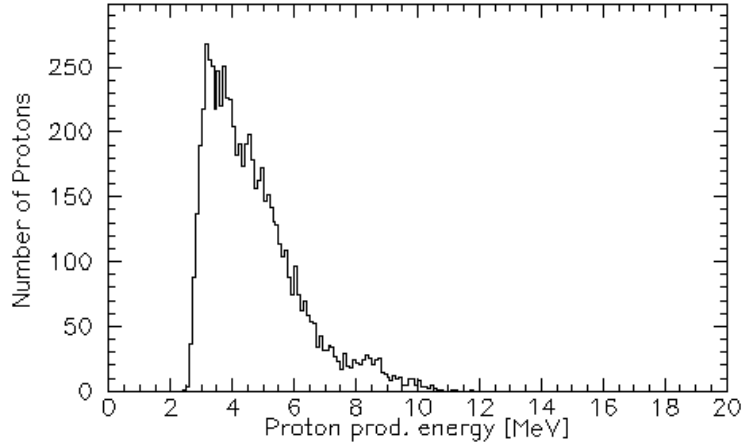
Figure 4.1: The calculated production energy of protons in the target foil.

we can calculate the angle that the proton was emitted with from the target foil in the laboratory system, and with this we can make a plot of particle production energy versus emission angle. Doing this for all particles we get the result seen in figure 4.2.

The proton spectrum can be seen in the upper left corner and we now clearly see structure. The spectrum seen in figure 4.1 corresponds to the projection on the y-axis in figure 4.2. Apart from the proton spectrum a clear structure is also visible in the deuteron and the triton spectra. For α-particles the situation is less clear. We speculate that this is due to a compound contribution, effectively drowning out any structure information from the αs. For this reason we have left out α-particles from the data analysis in the following.

With the production energy and the laboratory angles, together with the known beam energy, we can convert our angles to the center of mass system. Assuming now that all reactions are binary, such that they can be written in the familiar form ^{11}Be(d,p)^{12}Be, we can calculate the excitation energy in the produced ^{12}Be to get our excitation spectrum. This uses the fact that the Q-value for the reaction is $Q = 0.944$MeV.

4.2 The proton channel and the ^{11}Be(d,p)^{12}Be reaction

The excited states of ^{12}Be are not that well studied, although the nucleus has been getting more attention recently. We will go through the previous experimental knowledge of the ^{12}Be states below and also discuss what
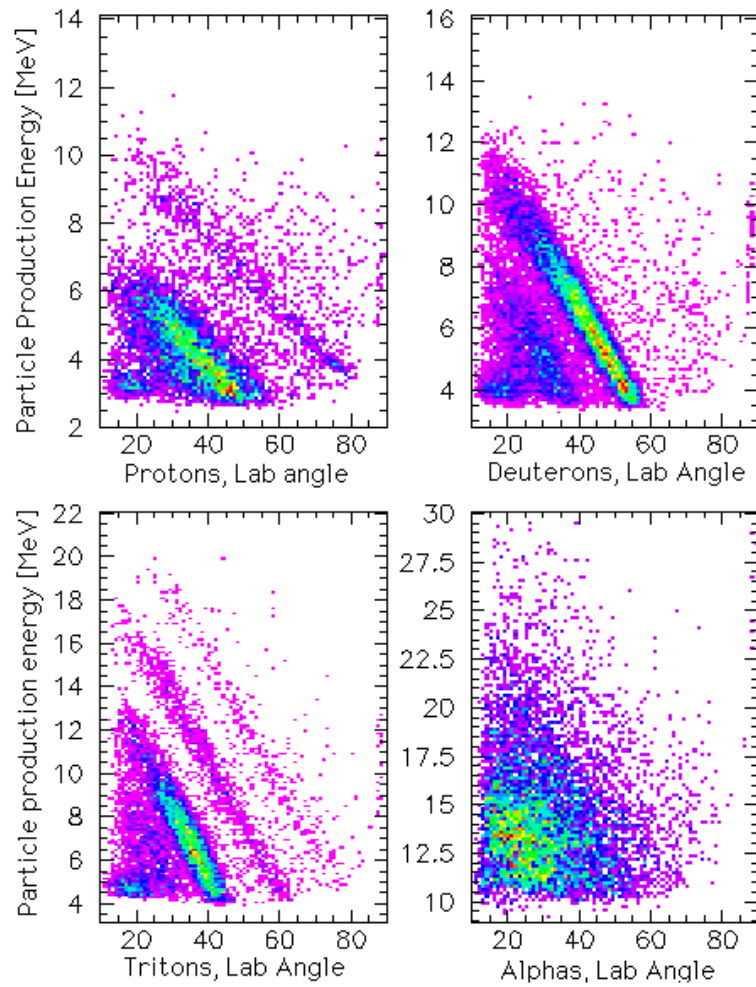
Figure 4.2: Spectrum showing the angular distribution of particles produced in the reaction. The energy on the y-axis is the energy the particle was produced with.

theoretical models consistently predict.

The ^{12}Be ground state properties, $J^\pi = 0^+$, were determined already in 1994 using a 17MeV triton beam and the reaction ^{10}Be(t,p)^{12}Be [54]. This experiment also saw the first excited state at 2.1 MeV, and determined its properties correctly to be $J^\pi = 2^+$. The state we now think is the third excited state was also seen in this experiment at 2.7MeV excitation energy, although it was suggested to have $J^\pi = 0^+$ instead of $J^\pi = 1^-$ which we now know to be correct.

The other states in ^{12}Be have only been observed very recently. The second excited state has been seen in a high energy collisions at RIKEN, produced by fragmenting a 100MeV/u beam of ^{18}O in a Beryllium target and observing angular correlated γ-transitions in coincidence with the ^{12}Be fragment [55].

The third excited state was seen in a very similar RIKEN experiment to the one above. This observation actually predates the second excited one [56]. The state was observed by scattering a beam of ^{12}Be of carbon and lead targets and observing de-excitation through γ-decay. The state was determined to have $J^\pi = 1^-$ in the same experiment. The experimental knowledge of states in ^{12}Be is summarized in table 4.1.

State	E_x (MeV $\pm$ keV)	$J^\pi; T$	From
gs	0	$0^+; 2$	[54]
1st	2.111 ± 3	$2^+; 2$	[54]
2nd	2.240 ± 20	0^+	[55]
3rd	2.680 ± 20	1^-	[56]
	2.730 ± 3	(0^+)	[54]

Table 4.1: Table of previously observed states in ^{12}Be together with the observed properties.

During the preparation of this thesis a newer paper investigating states in ^{12}Be, by the same authors as [55] and using the same reaction at RIKEN was found [57]. They identify the first and second excited states in the above table with slightly refined values for the excitation energies, but since the differences are only small we keep the values in table 4.1.

Modeling ^{12}Be in both ground and excited states have been approached in many different ways, these include anti-symmetrized molecular dynamics [47] for the highly excited states, but also shell model [48, 49] and three-body models based on a core of ^{10}Be and two neutrons have been used [50, 51, 52]. A very recent three body paper, actually predicts a new, previously unobserved, 0^- particle bound state that should be within the reach of our experiment [53].
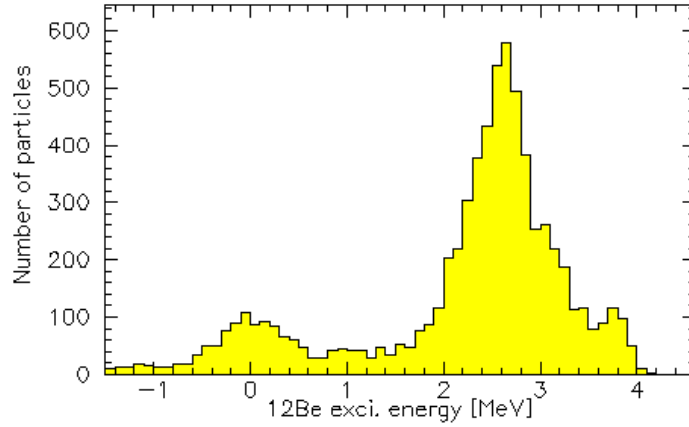
Figure 4.3: The ^{12}Be excitation spectrum.

The different models differ somewhat in the predicted spectra, but agree that one consequence of the breaking of the $N = 8$ magic number is the appearance of a low lying 0^+ state, which we see in table 4.1 as the second excited state. Many, but not all, models also predict a 1^- state below the neutron threshold, at 3.17MeV. The state seen as the third excited state in [56] has these exact properties. An interesting observation was made in [52] namely that the three-body models that place the two outer neutrons in $s_{\frac{1}{2}}$ and $p_{\frac{1}{2}}$ orbits naturally predict a spectrum with excited 0^+, 1^- and 2^+ states. Since these states are all experimentally very close to the neutron threshold this could suggest that binding energy effects play a role in the structure of theses states, possibly giving them halo character. On the other hand other models include contributions from the $d_{\frac{5}{2}}$ orbit or excited core contributions [44]. The question of halo structure must therefore be answered experimentally.

4.2.1 Excitation energy of ^{12}Be

With everything presented in the previous two sections we are now ready to present the excitation spectrum obtained from our data. This can be seen in figure 4.3.

A number of features are immediately clear from this spectrum. First and foremost we do not resolve the excited states, but we see a clear feeding to the region that contain all of them. We also clearly see the ground state. We have some protons coming from other reactions than the binary ^{12}Be+p channel giving us 20-40 counts in each bin between the ground state and the first excited. A clear resolution of the three excited states was not expected with the current setup. The main goal was to get an overview of which

channels were fed in the reaction.

Another feature of the spectrum is that we see significant feeding above 3MeV, which at least suggest that perhaps another state could be present here. This would be very interesting in light of the recent three-body prediction of a new excited state [53]. To try and clarify the situation somewhat we turn to our simulation software.

4.2.2 Simulation

As mentioned already in chapter 3.1, we use simulations to help interpret our data, and to correct for angular detection efficiencies. We will take a look at both of these aspects below.

The first step in our simulation effort is to attempt the reproduction of the excitation spectrum to see if we can explain the observed structure solely by know states. This means that we input the excitation energies from table 4.1 in the simulation code and try to fix the feeding of different states by hand to reproduce the spectrum as best we can. We assume that all states have a delta shape, and so any broadening of the states is due to experimental effects, e.g. detector smearing or finite beam spot. The values we have used for the simulation of the ^{12}Be excitation spectrum can be seen in table 4.2.

State	E_x (MeV)	Branching %
gs	0	12.5
1st	2.111	7.5
2nd	2.240	13
3rd	2.730	41
4th	3.740	26

Table 4.2: Simulated excitations energies and branching ratios of states in ^{12}Be. Note that an extra state has been added in order to get any feeding above 3.2 MeV in the spectrum.

The excitation spectrum produced is slightly more skewed to show the effect that the branching ratios have on the shape of the spectrum. The state added at 3.74 MeV does not correspond to any known state in ^{12}Be. The next state has been seen at 4.5MeV [54]. This is included to populate this part of the spectrum. The extra feeding at high energy could also be caused by protons from other reactions that are being wrongly identified when assumed to be from the binary reaction ^{11}Be(d,p)^{12}Be.

The simulation shows that it is possible to make an educated guess regarding the distribution of states but not on a scale that would be useful for any real physics calculation. To resolve the different states, in a future
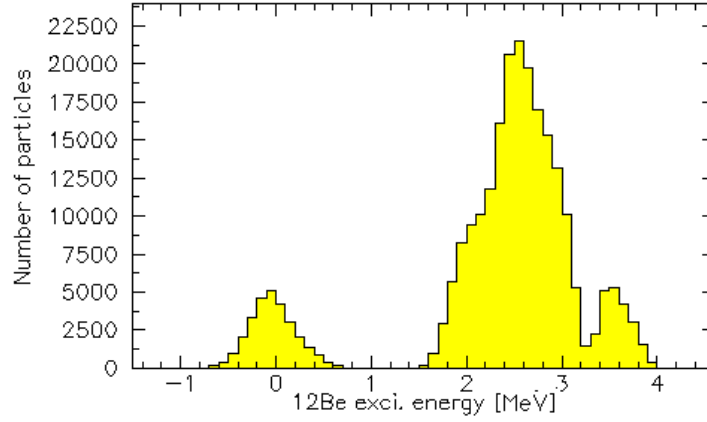
Figure 4.4: The simulated ^{12}Be excitation spectrum.

experiment will require γ-detectors such that the decay of the states could be detected in coincidence with the charged particles. We will return to this future possibility in section 4.6.

The next step in our analysis is to look at the angular distribution of particles in the center of mass system. To get the correct relative values between different angles, we need to correct for the angular acceptance of our detectors Not all angles are treated equally in square DSSSDs. For this purpose we assume that each state has a uniform angular distribution, and then use the obtained simulation distribution to correct our experimental spectrum. We will give an example below.

For this channel we divide our excitation energy spectrum into two parts, one containing the ground state and one containing the rest of the states. The ground state is defined as excitation energies between -0.66MeV and 0.80MeV, while the structure containing the other states is defined as energies between 1.65MeV and 3.75MeV.

4.2.3 Back to data, angular distributions

The angular distribution of our raw data can be seen as the upper panel in figure 4.5. The simulated spectrum, assumed to be uniform, can be seen in the middle as it has been detected. The corrected spectrum, the data divided, bin by bin, by the simulation, can be seen in the bottom. It is worth noting that there is a significant statistical error on the lowest angle bin from the simulation result.

A technical remark should probably be made at this point; the angles in figure 4.5 are reversed when compared to the normal convention on what
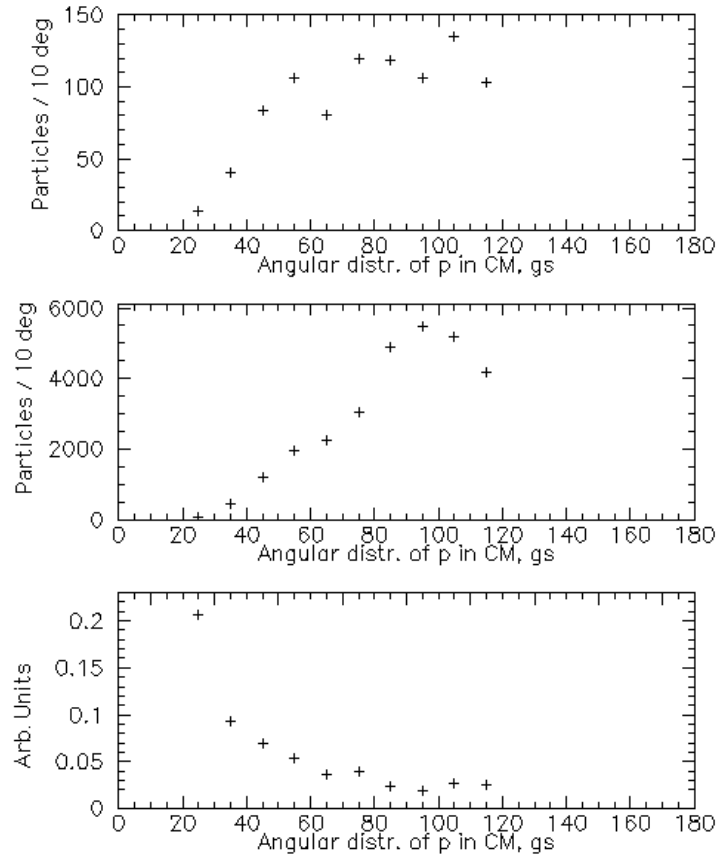
Figure 4.5: Top: Angular distribution of protons, corresponding to the ground state of ^{12}Be. Middle: Angular distribution of simulation data for the same state. Bottom: Data divided by simulation to correct for efficiency, but not yet converted to cross-section. This is the physical distribution. Note that the statistical error on the lowest angle bin is considerable. Note that all angles are reversed from the usual convention.

constitutes 0° and 180° in a reaction experiment[1]. This is a remnant in our analysis of the fact that our experiments take place in inverse kinematics, the center of mass system more or less follows the beam particle. This is thus the natural way to treat angles.

The lack of an absolute normalization restricts our ability to calculate an absolute value for the cross section. We are thus restricted to the arbitrary scale presented in figure 4.5 and all following angular distribution figures. It is worth noting that all angular distributions are on *the same* arbitrary scale, and so relative cross sections can still be inferred from the figures presented here and in the following. Section 4.5 has more details on attempts to obtain an absolute normalization for the data.

Our lack of normalization also restricts our ability to place meaningful error-bars on our data since the normalization error will be a significant error-source. The statistical error on the data in this and the following is of the order of 5% for the most populated states, but significantly larger for the outer lying states which are only weakly fed.

The final remark we will make concerning the angular distribution spectra is that the most structure information can be inferred from the way the distribution behaves at small angles. Unfortunately the detector that broke during the experiment was the one placed at very low angles, and so this data was lost. However in a future experiment we should be able to get reliable data down to 5°-10° in the center of mass system.

The final piece of data we will present before we move on to the next channel is the angular distribution of the combined structure comprising all the excited states in ^{12}Be. This can be seen in figure 4.6. It was labeled "1st excited" in the analysis for easy identification since it is the first structure apart from the ground state that is seen. The same convention is used for the other distributions. Not a lot can be inferred from this since it comprises so many states.

4.3 Elastic deuteron scattering and the ^{11}Be(d,d)^{11}Be* reaction

The elastic channel in the ^{11}Be+d plays a minor, but still important, role in our investigation.

As mentioned already in the introduction to this chapter, ^{11}Be has a very famous one neutron halo in both the ground and first excited state, which is situated just 320keV above the ground state as seen in table 4.3. This makes it a unique nucleus in the sense that it can decay via an E1 transition from one halo state to another. While the effect is at this point well understood, we would still like to study how this affect reactions taking place at our ISOLDE energies in the future.

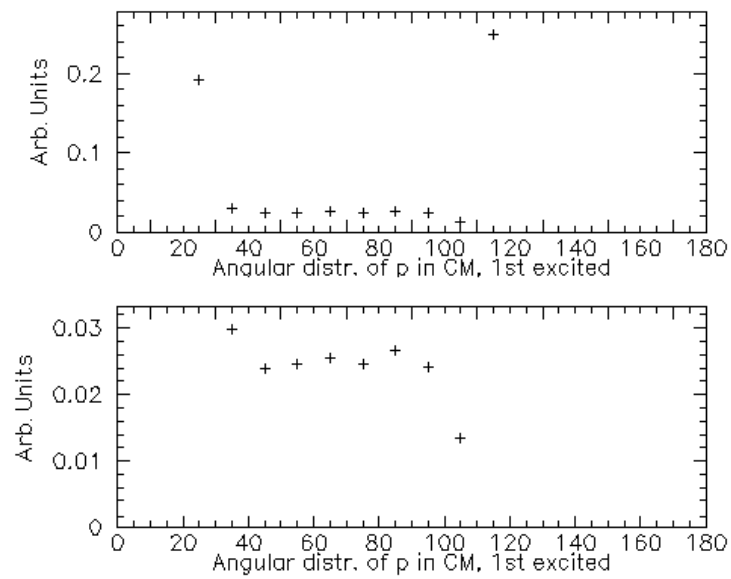[1]In our plots 180° is the incoming beam direction

Figure 4.6: The angular distribution of protons in the structure containing everything but the ground state, labeled the 1st excited group. The upper panel is the corrected values, corresponding to the bottom panel in figure 4.5. The bottom panel has had the two outer points removed since their statistical error was very large. Note that both of these plots are on the same scale as the bottom panel of figure 4.5.

State	E_x (MeV $\pm$ keV)	$J^\pi; T$
gs	0	$\frac{1}{2}^+; \frac{3}{2}$
1st	0.32004 ± 0.1	$\frac{1}{2}^-$
2nd	1.778 ± 12	$(\frac{5}{2}, \frac{3}{2})^+$

Table 4.3: Table of previously observed states in ^{11}Be together with observed properties. From [62].

The pure elastic part of the reaction plays a very important role for the theoretical description as it can be used as the basis for a Continuum Discretized Coupled Channel (CDCC) calculation. Unfortunately, an optical model fit to the ground state diverges due to the very low lying first excited state [58]. Thus an absolute normalization of our spectra is needed to fix this divergence before any attempt can be made to model the rest of the channels using the CDCC formalism.

^{11}Be is also interesting due to the possible existence of dipole polarizability. In a strong electrical field this effect would cause the positively charged ^{10}Be core to move in the direction of the field, relative to the center of mass, and the halo neutron to move in the opposite direction. Dipole polarizability should strongly effect the elastic scattering of halo nuclei on heavy targets, even at low energies, and thus be measurable at ISOLDE [59].

The effect has been observed previously in the double neutron halo nucleus ^{6}He in an experiment at Louvan-Le-Nouvre in Belgium[61], and possibly a hint of it has been seen at GANIL in ^{11}Be at beam energies significantly higher than REX-ISOLDE [60]. We do not expect to observe the effect in this experiment, but it could be interesting for the future.

The excitation spectrum we obtained for ^{11}Be can be seen in figure 4.7. We clearly see a structure containing the ground and first excited state, and it is very clear that we do not resolve these two states. However, an absolute normalization would open the door for a theoretical attempt at separating the two. As with the states in ^{12}Be, these could also be resolved using γ-spectroscopy. The second excited state is seen clearly isolated around 1.9MeV in the excitation spectrum as was to be expected.

4.3.1 Simulation

The simulation for this nucleus was rather simple since we only populate three states, and only resolve them into two different groups. Since the ground state and first excited are so close, we have not included the 320keV state as an independent state in the simulation. The energies and branching ratios used can be seen in table 4.4.

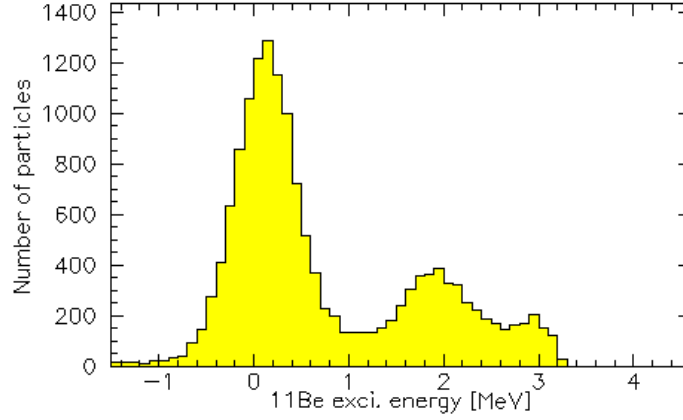With the values from the table the simulated excitation spectrum can

Figure 4.7: The measured ^{11}Be excitation spectrum.

State	E_x (MeV)	Branching %
gs	0	70
1st	1.850	30

Table 4.4: Simulation values for excitation energies and branching ratios for states in ^{11}Be. Note that the ground state and the 320keV excited state are treated as one in the simulation.

be seen in figure 4.8. We see that we nicely reproduce the two structures seen in the spectrum. The data above 2.5MeV in the excitation spectrum in figure 4.7 does not seem to be from a state in ^{11}Be and could be from misidentified protons coming from reactions other than ^{11}Be(d,d)^{11}Be*.

4.3.2 Angular distributions and theoretical modeling

As was the case with the ^{11}Be channel, we now use the simulation data to construct acceptance corrected angular distribution spectra for the two structures. The ground state is again defined as excitation energies between -0.66MeV and 0.8MeV. The corrected angular distribution can be seen in figure 4.9. Apart from the first bin which has a high statistical uncertainty, we actually see a nice structure for the ground and first excited state peak.

The second excited state (first excited group) is defined as energies between 1.30MeV and 2.41MeV, and the corrected spectrum can be seen in figure 4.10. Again the first bin has very low statistics and thus a very high statistical error. The rest of the spectrum does not show significant structure. This is consistent with what is expected. Interesting data would be at
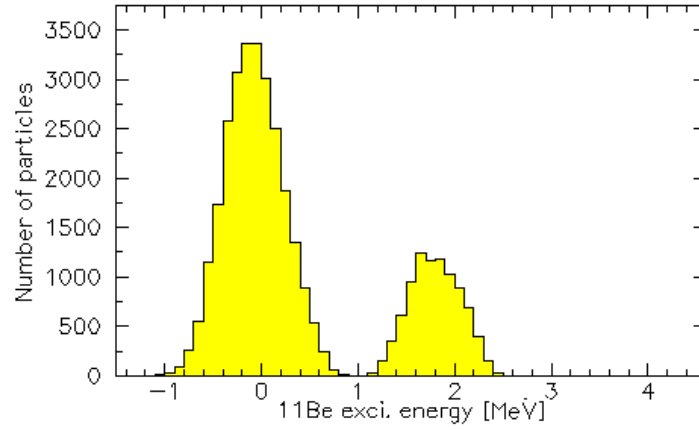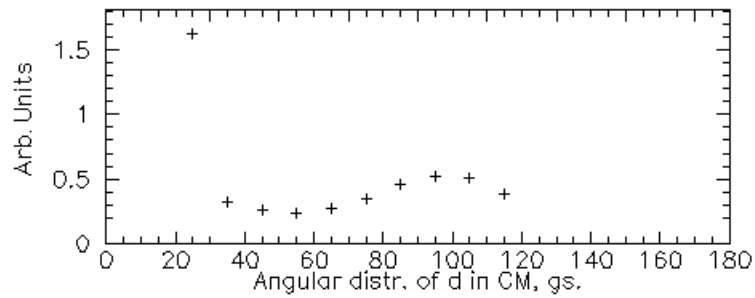
Figure 4.8: The simulated [11]Be excitation spectrum.

Figure 4.9: Angular distribution of the ground state group, containing the ground state and first excited state, in [11]Be.
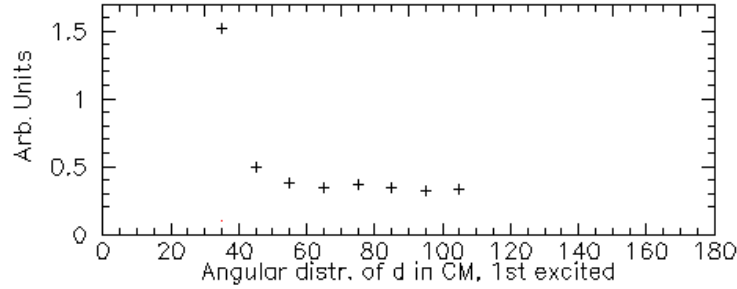
Figure 4.10: The angular distribution of the first excited group in ^{11}Be.

more extreme angles where we unfortunately do not have data.

As already mentioned above it is very difficult to model the ^{11}Be(d,d)^{11}Be scattering without an absolute normalization. In figure 4.11 our combined ground and first excited state angular distribution has been scaled for comparison with data from the reaction on ^{11}B as well as an optical potential. It is clear that the same general features are present for angles between 60° and 140°, and this might indicate that the same optical potential would describe the two different scattering reactions. However, since the data has been scaled to fit, nothing can be said of the absolute cross section values. Notice that the angles in this figure have been transformed from our inverse kinematics angles to regular scattering angles.

4.4 The triton channel and the ^{11}Be(d,t)^{10}Be reaction

The last reaction channel in our experiment that yielded interesting data was the triton channel populating states in ^{10}Be. This is a rather well-known and well studied nucleus, and so we do not expect to be able to extract much new structure information. It will mainly serve to verify our calculations on the other channels. With that said however, the data does look rather interesting.

The known states in ^{10}Be within our reach are given in table 4.5 along with their properties. The Q-value of the ^{11}Be(d,t)^{10}Be reaction is 5.75MeV. Two states are particularly interesting, and those are the two negative parity states around an excitation energy of 6MeV. The reason is that they are relatively close to the one neutron binding energy of $S_n = 6.81$MeV and that their spin-parity could correspond to the ^{9}Be ground state coupled to an $s_{\frac{1}{2}}$ neutron. Both of these states are thus possible one neutron halo states.

If this is indeed the case, the transfer reaction from the ^{11}Be halo to
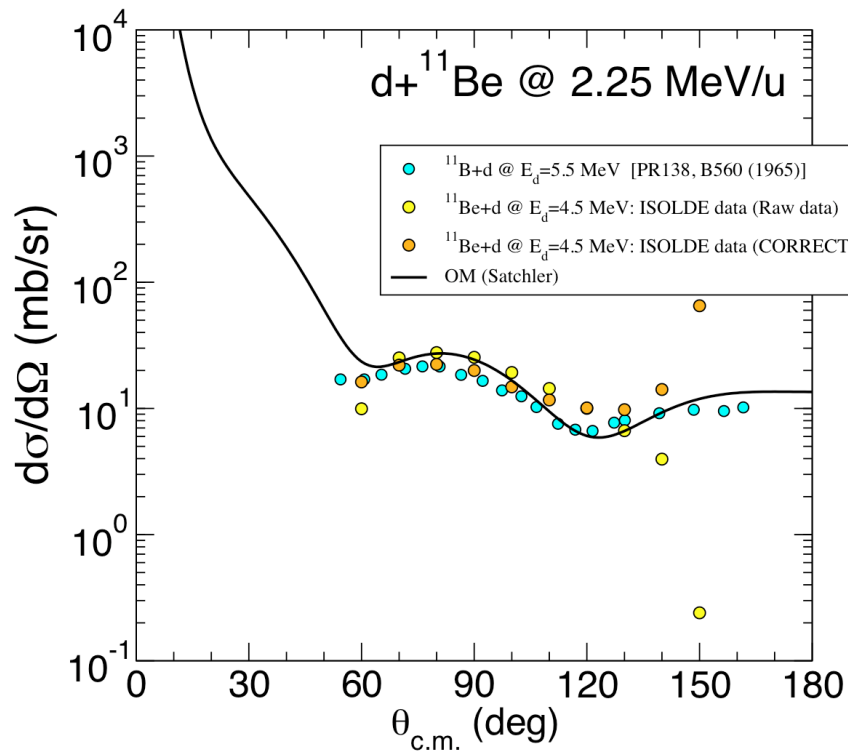
Figure 4.11: An optical model potential placed on top of our ^{11}Be data, both in the raw data form and the corrected values. Along with ^{11}B+d data and all scaled to fit on the same figure [58]. Note: Angles on this plot have been *reversed*.

E_x (MeV)	$J^\pi; T$
0	$0^+; 1$
3.36803	$2^+; 1$
5.95839	$2^+; 1$
5.9599	$1^-; 1$
6.1793	$0^+; 1$
6.2633	$2^-; 1$
7.371	$3^-; 1$
7.542	$2^+; 1$

Table 4.5: Table showing the properties of the relevant states in [10]Be. From [63].

the [10]Be halo would be very interesting to study and would be available at ISOLDE. It is possible this transfer has already been seen at much higher energy in [40], but it is not immediately clear from the article.

The excitation spectrum from this experiment can be seen in figure 4.12. It is interesting that the ground state is only barely populated, while the highly excited states are much more so. Naively one would expect a neutron pick-up from the [11]Be-halo by the deuteron to be a likely event, leaving the [10]Be core unperturbed. However, this does not seem to be the case. One reason for this might be the high Q-value of the reaction, but further theoretical modeling will be needed to understand this.

4.4.1 Simulation

As with the other channels the excitation spectrum for [10]Be was simulated using an appropriate number of excited states. As a number of the higher exited states are spaced very closely, they have been grouped. The excitation energies and branching ratios used in the simulation can be seen in table 4.6.

With the values in the table the simulated excitation spectrum can be seen in fig 4.13.

It is clear that the simulation reproduces the experimental spectrum very well for excitation values lower than 8MeV. It is also clear that even though we have put in two excited state with excitation energies close to 9MeV, no feeding is seen in the simulation above 8MeV. Consequently, the tritons seen experimentally cannot be from the [11]Be(d,t)[10]Be reaction.

One possibility, and the most likely one, is that these tritons are from the disintegration of [12]B in the two step process [11]Be+d→[12]B+n followed by [12]B→[9]Be+t. The Q-value of this reaction is $Q = -1.06$MeV, and so it is well within range. However. it will produce lower energy tritons compared

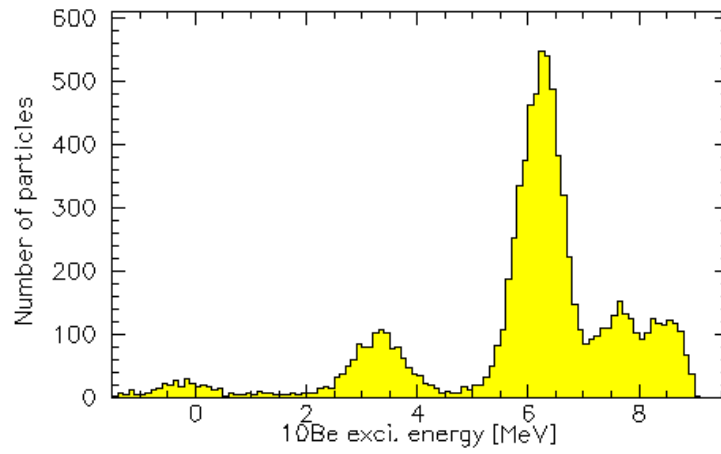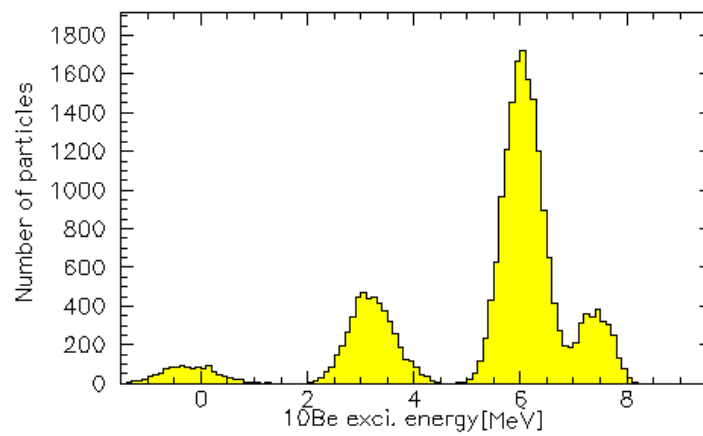Figure 4.12: The measured ^{10}Be excitation spectrum.

Figure 4.13: The simulated ^{10}Be excitation spectrum.

State	E_x (MeV)	Branching %
gs	0	3
1st	3.368	12
2nd	5.960	8
3rd	6.200	22
4th	7.371	2
5th	7.542	8
6th	9.270	5
7th	9.450	30

Table 4.6: Simulation values for excitation energies and branching ratios for states in ^{10}Be. Note that some of the closer-lying states in table 4.5 have been merged into one in the simulation. Also the two states above 9MeV was an attempt to populate states above 8MeV as seen in the data in figure 4.12. See the text for details.
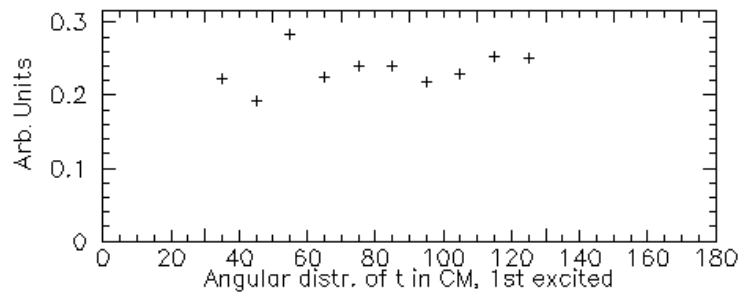
Figure 4.14: The angular distribution of the first excited group, in this case also the first exited state, in ^{10}Be.

to the ones from ^{11}Be(d,t)^{10}Be with Q =5.75MeV. This fits well with the fact that low energy tritons will be translated into high excitation energies in ^{10}Be.

It is possible that a similar effect is responsible for the small structure seen just under 4MeV in figure 4.3.

4.4.2 Angular distributions

As with the other data we have constructed angular distribution plots for all the discernible groups of excited states. The first group in this case is actually also the first excited state and has been defined as excitation energies between 1.90MeV and 4.2MeV. The distribution can be seen in figure 4.14 and does not show a great deal of structure.

Figure 4.15: The angular distribution of the second excited group state in the ^{10}Be spectrum.

Figure 4.16: The angular distribution of the third excited group in in the ^{10}Be spectrum.
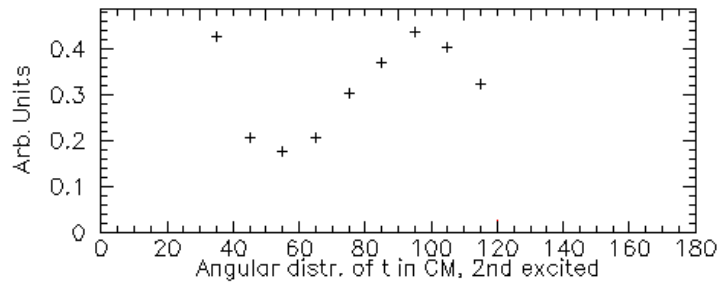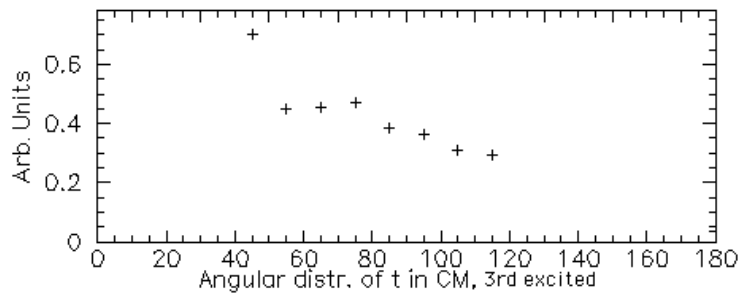
The second group is defined as energies between 5.30MeV and 6.8MeV. Referring to table 4.5, it should thus contain no less then four different states. The distribution can be seen in figure 4.15. Perhaps surprisingly for such a diverse collection of states, the distribution shows a great amount of structure. This might be due to one or a few states dominating this group, but further analysis and possibly resolution through γ-detection will be needed to clarify this. Note, however, that l-values will be different for transfer to the negative parity states opposed to the positive parity states. It would be very interesting if the first transfer reaction dominates.

The third group, defined as energies from 7.1MeV to 7.9MeV, is the final group we have looked at since we do not feed states above 8 MeV in the simulation. According to table 4.5 this region should contain two excited states. The resulting distribution can be seen in figure 4.16. It is very difficult to say whether or not this spectrum contains something useful without theory input. To the optimist it certainly contains something that looks like structure, but on the other hand the sceptic may justifiably be, well, sceptic.

4.5   Absolute normalization

The analysis presented in this thesis is only preliminary and further work will be needed to extract all available information. One key thing that is missing is an absolute normalization to allow for calculation of absolute cross sections and CDCC calculations. The following procedure is an attempt to normalize these data, but unfortunately the implementation has left us with values that we do not trust when compared to ^{11}B+d in figure 4.11.

In order for us to calculate absolute cross sections from our data we need to estimate the rate of ^{11}Be in the chamber. This is not at all trivial since the design of ISOLDE and REX leads to natural long and short term fluctuations in the beam intensity. Long term fluctuations arises e.g. from the gradual break down by the protons of the primary target, while fluctuating proton intensity, both in the amount of pulses that impinge and the number of protons in a pulse, creates both long and short term fluctuations due to target heating and the simple fact that fewer protons produce fewer interesting nuclei.

We work around this by averaging the short term fluctuations while avoiding the longterm ones. What we do is to use a silver target of a known thickness placed at the target position to estimate the rate of ^{11}Be since the Rutherford cross sections is very well known. We then switch to our deuterated polyethylene target and assume the position and the rate stays the same. This then gives us our normalization. The technique was invented during our experiment, and we consequently have very little silver data in our data set.

To verify the validity of this technique, we need to show that the short term fluctuations average out, and that we can get enough data without being hit by long term ones. To do this, a time resolved histogram of the rate of ^{11}Be has been produced and can be seen in figure 4.17. The figure shows all of our usable silver data.

Producing this figure is not trivial, since our events have no timestamp. Time resolution is achieved though a cunning technique using our setup and the DAQ trigger settings. As we saw in section 2.2, the REX beam is bunched and pulsed. The frequency of REX-pulses is 50Hz but the bunch-length is only 200μs, and so the time between bunches is relatively long. In order to avoid dead-time, the EBIS release signal was used as an extra trigger in our DAQ in order to start with a "clean slate" when particles arrive. We thus have non-Be events with a special trigger code. Detector triggers are trigger type 1, while EBIS-triggers are type 4. Since the EBIS is closed, and has been so for a long time when a new bunch is released, virtually all of the EBIS-trigger events are in the data-stream. This means that even though we have no timestamp on our events, we effectively have a 50Hz clock in our data-stream. By counting EBIS-triggers we can time-resolve our events and correspondingly get reaction rates.
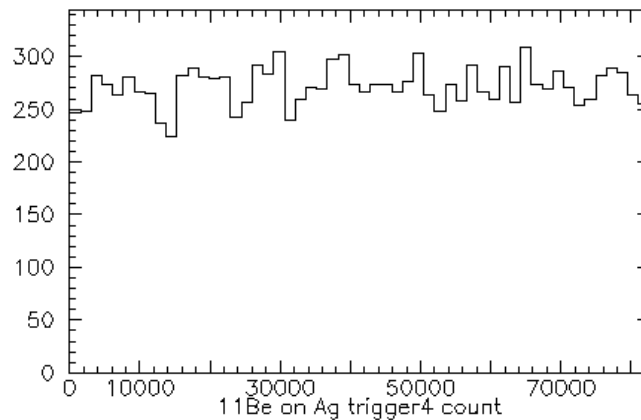
Figure 4.17: ^{11}Be seen in DSSSD2 versus EBIS trigger (Trigger 4) count. EBIS trigger functions as a 50Hz clock, see section 4.5 for details. The binning corresponds to 30 seconds of data.

In figure 4.17 we clearly see the short term fluctuations in the ^{11}Be rate. The data in the figure has been taken over 27 minutes and the binning corresponds to 30 seconds. Integrating the first and second half of the data gives correspondingly 7288 and 7361 events, a difference of around 1%. It thus seems safe to assume that the fluctuations even out on this time-scale.

The second part of our normalization effort is to look at deuteron data. Using the same technique as described earlier, a plot of the number of deuterons detected as a function of time has been produced and can be seen in figure 4.18.

It is clear that the fluctuations in this figure are a lot larger than the ones seen in figure 4.18. At least part of this is explained by the lower statistics giving relatively larger fluctuations. The amount of exit channels for this reaction is also a lot larger than the simple Rutherford scattering from before. The data in figure 4.18 has been taken over 88 minutes and the binning is again 30 seconds. If we again average over the first and second half of the data we find that the number of events is 4182 and 3741 correspondingly, a difference of just over 10%. It would thus seem that we should be able to normalize our data to an accuracy of 10%.

4.6 Conclusions

Even though this experiment was exploratory in nature, we have learned that it is possible to use a ^{11}Be reaction to study the structure of ^{12}Be at an ISOL post-accelerator. Furthermore, once we get absolute normalizations, the cross sections to the different groups of states can be determined. With
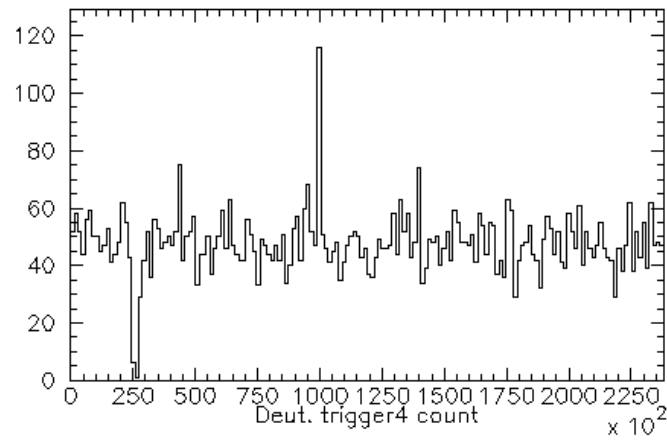
Figure 4.18: The amount of deuterons seen in DSSSD2 versus EBIS trigger (Trigger 4) count. This corresponds to figure 4.17 and also has 30 second binning.

help from theoretical models we may even be able to resolve individual states. This means that despite our limited resolution we do expect to be able to extract at least some structure information from the data.

Also from this study we have learned sufficient to be able to plan the next stage, which will aim to add γ-detection in coincidence with charged particles. This will most likely be by using the Mini-ball 4π γ-detector already present at ISOLDE. With the Mini-ball we should be able to resolve all the states in ^{12}Be as well as determine their properties. Should a new 0^+ exist, as suggested by some theorists, we expect to see that as well.

Also, adding γ-detection will allow us to easily differentiate between the ground state and the 320keV exited state in ^{11}Be which should ease our normalization and modeling efforts.

Chapter 5

A look at ^{11}Be+p

As mentioned in chapter 3 a proton foil was also placed on our target ladder, allowing us to look at the reaction ^{11}Be+p. This served several purposes in our experiment. In the original work on ^{9}Li+d a significant contamination of protons was found in the deuteron foil. Estimating this contamination would be easier with this data, should it exist in our foil as well. Also a comparison of the two pick up reactions ^{11}Be(d,t)^{10}Be and ^{11}Be(p,d)^{10}Be could be interesting, even though, ^{10}Be is a very well known nucleus.

The proton data was taken during the same run as the deuteron data, and so the experimental parameters, including all calibrations, are the same for the two data sets. The foil thickness was specified to be the same as the deuteron foil thickness. The only major difference between the proton foil data and the deuteron foil is the amount of time that each was observed. Roughly a factor of 10 less time was used on the proton foil compared to the deuteron foil.

5.1   Elastic scattering, the ^{11}Be(p,p)^{11}Be reaction

We have already specified the interesting points and relevant states in ^{11}Be in the last chapter, and so in this we will jump straight to the data. The excitation spectrum obtained from the experiment can be seen in figure 5.1.

The difference between this and figure 4.7 is striking for several reasons. Firstly we see no excited states in the proton scattering spectrum at all. Secondly the amount of statistics in the two spectra appear to be the same, and so the observed cross section for elastic scattering on protons is much higher than for deuterons. The third thing that is different is the width of the peak, which is significantly narrower in this channel. We shall touch on this point in the next section.

One final thing that is indicated by figure 5.1 is that there does not seem to be significant feeding to the 320keV excited state. This could not be resolved in figure 4.7 but is actually consistent with what is seen in a
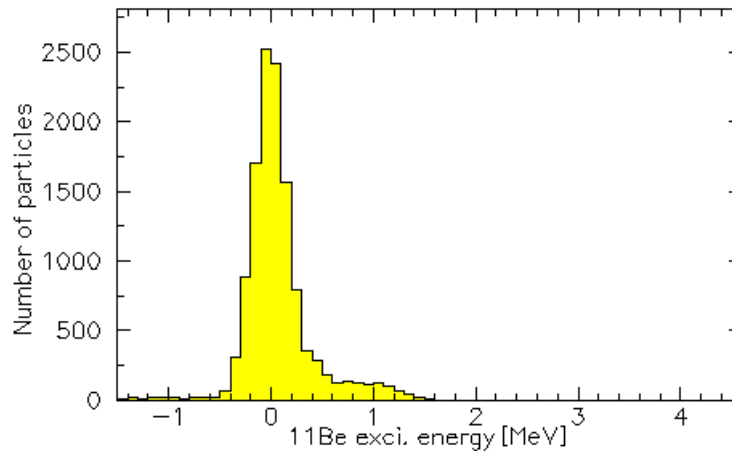
Figure 5.1: The measured ^{11}Be excitation spectrum from scattering of protons

similar reaction at higher energies in [60] where an analysis determines less than 10% feeding to the 320keV. Should the same somehow be the case for the deuteron reaction, modeling efforts would be helped greatly. We would then be able to use the same normalization method as in the ^{9}Li case [21]. Here data was normalized using the known elastic scattering cross-section.

5.1.1 Simulation and angular distribution

As with the deuteron data, we have used simulations to reproduce the excitation spectra. This case was particularly easy and so we will show no table of the used states. The resulting excitation spectra can be seen in figure 5.2.

We see that the simulated peak is as narrow as the one in figure 5.1, indicating that the width of this peak and the one in 4.7 is determined by kinematics that is well described in our simulation.

Again from the data and simulation an angular distribution plot was also constructed and can be seen in figure 5.3. If we ignore the two outermost points we see a very nice elastic scattering cross section.

5.2 The (p,d) pickup reaction, states in ^{10}Be

The one neutron pickup reaction ^{11}Be(p,d)^{10}Be should naively be similar to the ^{11}Be(d,t)^{10}Be one neutron pickup reaction seen in the last chapter. However, if we look at the excitation spectrum in figure 5.4 we see a big difference. Whereas almost all the feeding in the (d,t) reaction was to excited states and in particular the ones around 6-7 MeV, we only see the ground

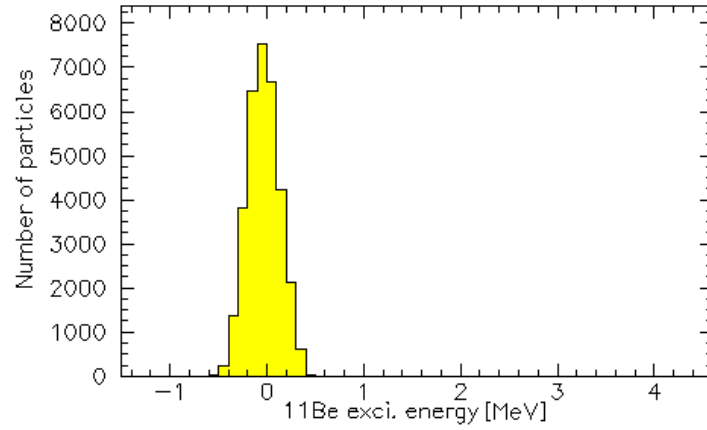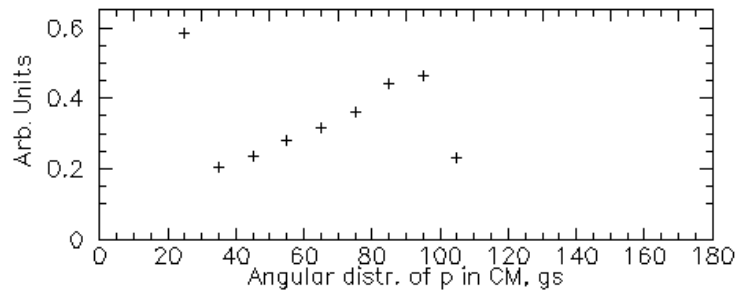Figure 5.2: The simulated ^{11}Be excitation spectrum from proton scattering.

Figure 5.3: The angular distribution of the ground state in the ^{11}Be spectrum from proton scattering. The two extreme angles have very high statistical errors.
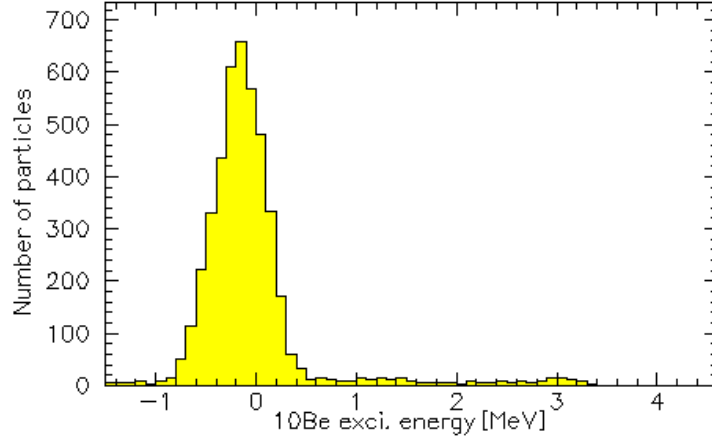
Figure 5.4: The ^{10}Be excitation spectrum from the proton reaction.

state in this reaction.

One major difference between the two reactions is the Q-value. In the (d,t) reaction it was 5.75MeV due to the strong binding of the second neutron in the triton. In the (p,d) reaction however the Q-value is only 1.72MeV. The second difference is that for such a light beam particle as ^{11}Be there is a significant change in the center-of-mass system for proton and deuteron targets. We can calculate the kinetic energy of the relative motion in the center of mass system for the two reactions using the formulas from [5]. For the deuteron case this gives

$$
\begin{aligned}
E_{\mathrm{cm}}^{\mathrm{d}} & = \frac{m_{\mathrm{d}}}{m_{\mathrm{d}} + m_{^{11}\mathrm{Be}}} E_{^{11}\mathrm{Be}} \\
& = \frac{2\mathrm{u}}{2\mathrm{u} + 11\mathrm{u}} (2.25\mathrm{MeV/u} \cdot 11\mathrm{u}) = 3.81\mathrm{MeV},
\end{aligned}
$$

while in the proton case we get

$$
\begin{aligned}
E_{\mathrm{cm}}^{\mathrm{p}} & = \frac{m_{\mathrm{p}}}{m_{\mathrm{p}} + m_{^{11}\mathrm{Be}}} E_{^{11}\mathrm{Be}} \\
& = \frac{1\mathrm{u}}{1\mathrm{u} + 11\mathrm{u}} (2.25\mathrm{MeV/u} \cdot 11\mathrm{u}) = 2.06\mathrm{MeV}.
\end{aligned}
$$

The change in the center of mass system thus greatly changes the energy available for the reaction. If Q-value and kinetic energy are added we see that for the (d,t)-reaction we can reach states up to around 9.6MeV while for the (p,d)-reaction we can only go up to 3.4MeV. This means that we can barely reach the first excited state in ^{10}Be at 3.37MeV. If we take into account that deuterons from this state will still have to be detected, which means passing
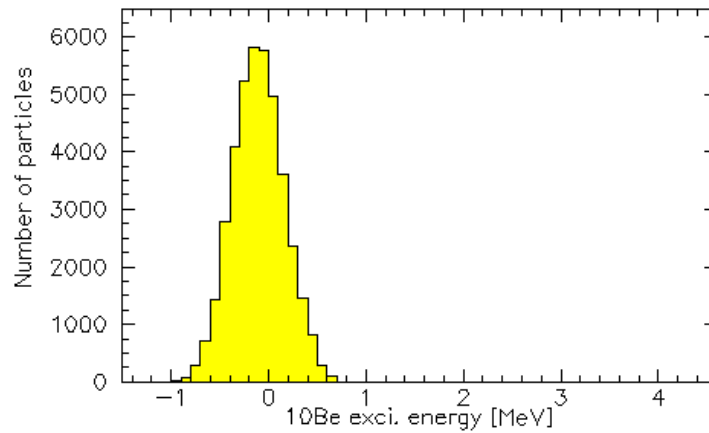
67

Figure 5.5: The simulated ^{10}Be excitation spectrum from the proton reaction.

through the Δ-detector requiring at least 2MeV kinetic energy, we see why no excited states are seen in the spectrum.

The last thing that is noteworthy in this spectrum is the intensity difference when compared to the (d,t)-reaction. The amount of statistics in the ground state peak is of the same order as the peaks in figure 4.12, but the amount of time on the proton target was still an order of magnitude less than the deuteron target. Part of this difference might be explained by the shift in detected center-of-mass angles. Part of it could also be explained by the faster center-of-mass movement changing the ΔE-penetration cut-off. But none of these will give us a factor of ten as observed.

5.2.1 Simulation and angular distribution

The simulated spectrum including only the ground state can be seen in figure 5.5 and we see that the ground state peak is nicely reproduced.

The angular distribution can be seen in figure 5.6 and does shows some structure. Again the outer angles should be ignored due to very low statistics before the correction.

5.3 The (p,t) pickup reaction, states in ^{9}Be

The final reaction we have included only for completeness. Since we also identify tritons in the proton data, we see states populated in ^{9}Be. The excitation spectrum can be seen in figure 5.7.

We see that we clearly populate the ground state and the first excited state. The properties of these two, as well as the second excited state barely
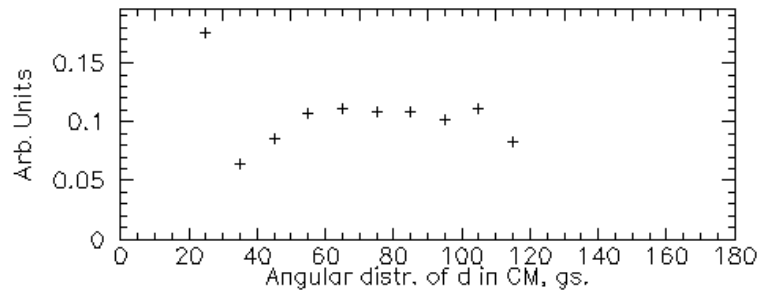
Figure 5.6: The angular distribution of the ground state in the ^{10}Be spectrum.
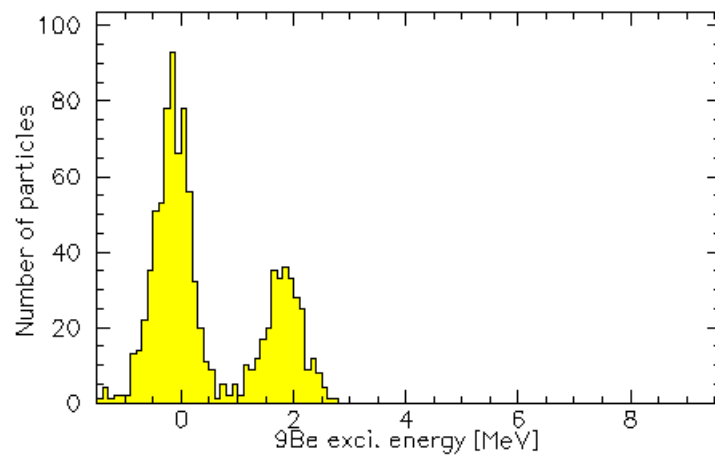
Figure 5.7: The measured ^{9}Be excitation spectrum from scattering of protons. Note the very low statistics in this plot.

within reach, can be seen in table 5.1. We can also note that we have very low statistics for this channel which would indicate that the two neutron pickup reaction (p,t) is not very efficient.

State	E_x (MeV $\pm$ keV)	$J^\pi; T$
gs	0	$\frac{3}{2}^+; \frac{1}{2}$
1st	1.684 ± 7	$\frac{1}{2}^+$
2nd	2.4294 ± 1.3	$\frac{5}{2}^-$

Table 5.1: Table of the three lowest lying states in ^{9}Be. From [63].

We have neither simulated this reaction nor made angular distributions, so with this final excitation spectrum we end our data analysis chapters.

Chapter 6

Detection of Low Energy Particles, DLEP

Part of my PhD has been funded by the European Union under the "Detection of Low Energy charged Particles"-program [64] and more than half a year has been spent in Spain working on this particular project. Most of the work presented in this chapter was done in close collaboration with John McGrath, University of York, while we were both in Madrid working at Consejo Superior de Investigaciones Cientificas (CSIC) and at Centro de Microanalisis de Materiales (CMAM) under encouraging supervision by Olof Tengblad.

The ability to detect and identify low energy charged particles is the cornerstone of the reaction and decay studies that have been and are being performed in our group and by our collaboration. Thus, as seen already in chapter 3. a great effort has been put into making our measurements as accurate as possible and our thresholds as low as possible. This has lead to the development of a range of techniques to describe loss effects in different parts of the setup, including the detector, and to the design of several new detectors. DLEP is the continuation of this search to lower our thresholds and increase the resolution in our experiments

The common feature of all our experiments involving DSSSDs is that they rely on traditional ΔE-E identification of particle as seen in section 3.6. This has the obvious limitation that a particle needs to penetrate the DSSSD and deposit energy in the active part of the thick detector behind it to be identified. Depending on the thickness of the DSSSD, this places a rather large low-energy cut-off on identification of even light charged particles. We have reprinted figure 3.10 above in figure 6.1, and the cutoff can be seen as the place where the "bananas" intersect the y-axis. We see that, in our case with 60μm of Silicon, for protons it is about 2MeV while for alphas it is around 9MeV. We can assume that the cutoffs are for particles hitting the detector at right angles. Hitting at an off angle would mean traversing more
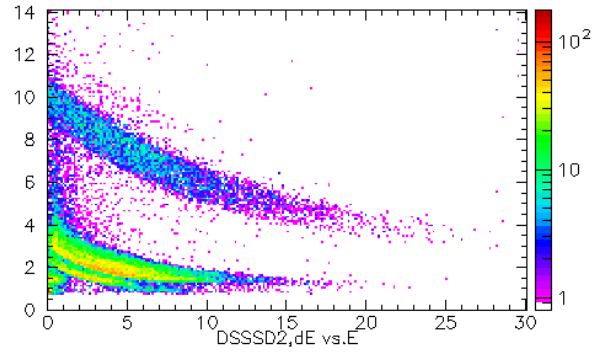
Figure 6.1: ΔE vs. E plot for data from ^{11}Be on deuterons, same as figure 3.10.
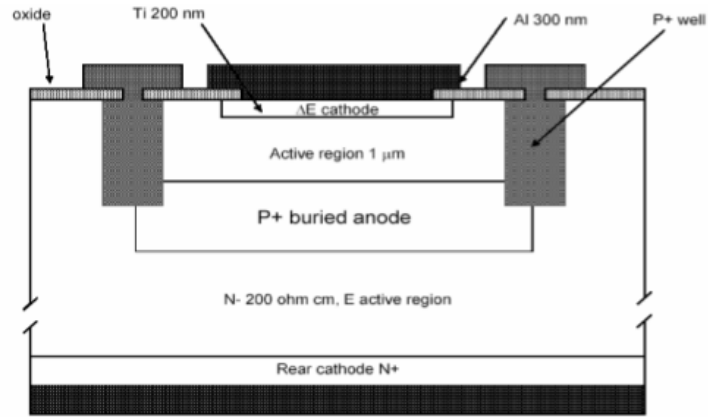
Figure 6.2: Drawing of the solid state components of the monolithic detector

of the detector and thus depositing more energy before penetrating.

The aim of DLEP is to keep the angular resolution working with segmented detectors while at the same time lower the threshold for identifying light charged particles. Two different strategies have been pursued in order to remedy the high cutoff. The first, which we will not cover in great detail, is the construction of a monolithic segmented detector which combines both ΔE- and E-part in a single solid state component. The design is very similar to the one presented in [65] but the size of the actual detector is much smaller. The thickness of the ΔE-part with this method can be significantly reduced to about 1μm, providing a significant reduction in threshold. The angular resolution is obtained by having 16 individual detectors on a single silicon component. The angular coverage of each single detector thus corresponds to an individual pixel of the old 16×16 DSSSDs, but the ac-
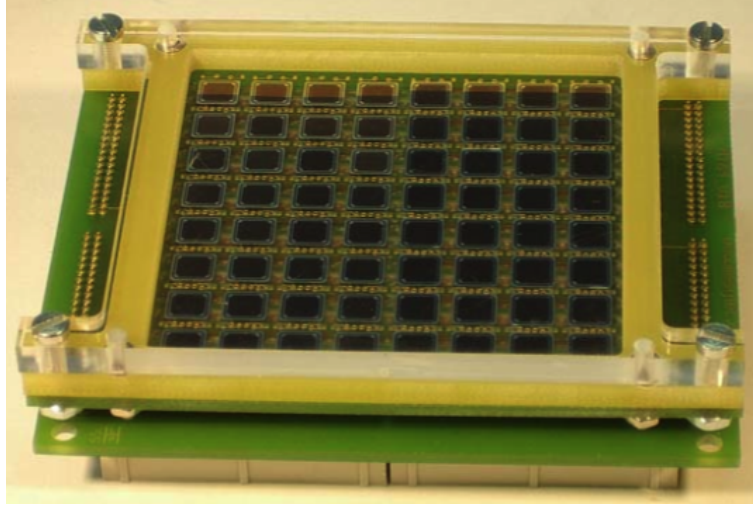
Figure 6.3: Picture of the constructed segmented monolithic detector

tual angular coverage is a lot smaller due to the gaps between individual detectors, leaving it with only 8×8 detectors.

Such a detector has already been produced by our collaborators in Gothenburg and is currently undergoing testing, a picture can be seen in figure 6.3. One advantage of this design is that traditional commercial electronics can be used, but the design does have several drawbacks. As mentioned, the angular coverage is significantly, naively 25%, smaller than for a corresponding DSSSD, but the biggest disadvantage is the amount of channels the detector needs in the electronics chain. A traditional 16×16 DSSSD needs 37 channels including the Si-pad E-detector, but the monolithic detector has 64 individual ΔE-E components and thus needs 128 channels, making it more cumbersome to work with. The final thing we will mention here is that it is not at all trivial how to calibrate the 128 channels for each detector.

The second strategy, the one to which I have contributed and the one we shall use the rest of the chapter on, is to construct an electronics device that will allow us to identify particles stopping inside our existing DSSSDs.

The idea, which we shall elaborate on below, is to analyze the shape of the electrical signals generated in the detector by each particle, and through that, identify the nature of the particle. This idea is not particularly new, it was first described in the 60's [66], but it is only recently that the advances in electronics [67] and fast high-resolution digitization circuits [68] has made the construction of such a system possible.

Pulse Shape Analysis (PSA) has already successfully been used for a number of different detector types, both for discrimination between gammas and neutrons in Ge-detectors [69], and for timing and identification of

charged particles in Silicon, [70] and [71], but at much higher reaction and particle energies than we operate at. Thus our challenge is to construct a system that will identify particles with an energy below 1 MeV stopping in 60μm of Silicon though PSA.

This turns out to be a rather elaborate piece of work. First we need to construct a system capable of capturing the pulse shape before we can try to analyze them and see if they contain any identifying features. We will cover the work done on both a capturing device, the preliminary work on an analyzing device as well as various other technical issues in section 6.2. First we will take a look at why we believe this might work.

6.1 The generation of signals in Silicon

Before we move into the more technical aspects, it is beneficial to outline a few characteristics of solid state, and in particular Silicon detectors. We have previously in chapter 3 looked at some of the specific challenges working with our DSSSDs, but a more general approach is needed in this section. The following section is heavily inspired by chapters 2, 4, 11 and Appendix D in [72].

At the basic level, our detectors work because any charged particle entering the detector interacts with the detector material. More specifically, the incoming nuclei interacts with the electrons of the detector, leading to excitation and ionisation of the detector material. This correspondingly removes kinetic energy from the incoming nuclei slowing and eventually stopping it, if there is enough detector material. Interactions between incoming nuclei and detector nuclei leading to Rutherford scattering or reactions, while possible, are sufficiently rare in our case to not play a role in the response of the detector.

The maximum energy that can be transferred by a particle with mass m and kinetic energy E to an electron with mass m_e in a single collision is $4Em_e/m$, or about 1/500 of the particle energy per nucleon. Because this is such a small number the incoming particle needs to interact with many electrons to stop. Since at any given time the particle is interacting with many electrons, the net effect is to lose energy continually through the detector material.

The effect of the particle stopping on the detector material is to leave a track of ionized atoms and free electrons, or in solid state physics terms, electron-hole pairs. The natural tendency for such pairs is to recombine to form neutral atoms, but by putting an electrical field over the detector these pairs can be extracted and measured. This gives us the simplified picture of a detector seen in figure 6.4

We will formalize this somewhat general approach to Silicon detectors in the next few pages, starting with how incoming charged particles are
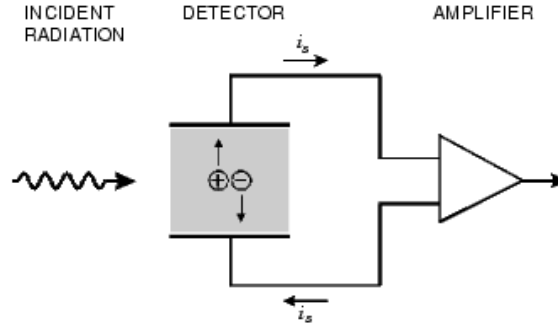
Figure 6.4: Very basic schematic of solid state detector.

stopped in an absorbing material.

6.1.1   Stopping Power

The linear stopping power S for a charged particle in any given material is defined as the energy loss per length of that particle in the particular material

$$S = \frac{dE}{dx}.$$ (6.1)

The value of S along a particle track is called the specific energy loss or rate of energy loss.

For an incoming particle with velocity v and charge state z the stopping power, S, increases as the velocity of the particle is decreased. The classical formula describing this is called the Bethe formula

$$-\frac{dE}{dx} = \frac{4\pi e^4 z^2}{m_e v^2} NB,$$ (6.2)

where

$$B \equiv Z \left[\ln \frac{2m_e v^2}{I} - \ln \left(1 - \frac{v^2}{c^2} \right) - \frac{v^2}{c^2} \right] \approx Z \ln \frac{2m_e v^2}{I}$$ (6.3)

and where the last step in eq. 6.3 is due to the fact that we work with non-relativistic particles. The parameters N and Z are the number density and the atomic number of the absorbing atoms respectively, m_e is the electron rest mass, and e the electron charge. The parameter I is the average excitation and ionisation potential of the absorber, and is usually treated as an experimentally determined parameter for each element.

Since eq. 6.3 changes slowly with incoming particle velocity, $B \propto \log v$, the overall behavior of eq. 6.2 with respect to v will be $1/v^2$. For a fixed absorbing material, say Silicon, the stopping power depends directly on the
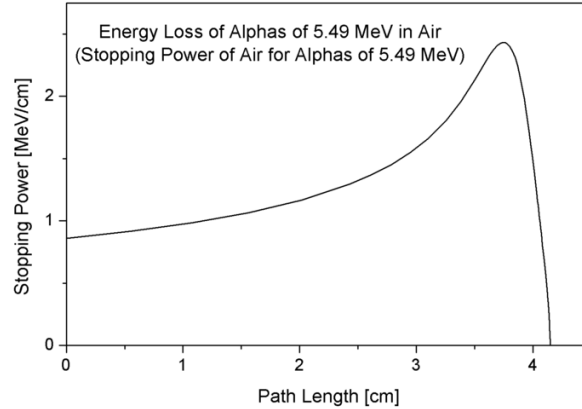
Figure 6.5: Illustration of a Bragg curve, here an α-particle stopping in air. From [73]

charge as z^2, and for two particles with the same kinetic energy indirectly on the mass of each particle through the dependence on $v^2 = 2E/m$. Thus particles with a greater charge will lose more energy than those with lower, and heavier particles will lose more than lighter ones.[1]

The expression in eq. 6.2 is valid as long as the velocity of the incoming particle is much bigger then the velocity of the electrons in the absorbing atoms. At low energy the incoming nuclei will pick up extra electrons and thereby change their charge state and the characteristics of stopping. Furthermore, at low ion velocity collisions may become adiabatic which also decreases the energy loss.

Plotting $-\frac{dE}{dx}$ versus the penetration depth in a stopping material gives us what is called a Bragg curve. An example of a several MeV α-particles stopping in air can be seen in figure 6.5. We see that initially the stopping goes as $1/E$ as expected, but near the end falls of as the α picks up electrons.

The curve shown in figure 6.5 is for a single particle. Due to the stochastic nature of the collisions the average energy loss of incoming α-particles will be different from that of any individual particle. This effect is called straggling and results in a natural spread of energies after a beam of mono-energetic particles has passed through an absorbing material.[2]

---

[1]This is exactly what enables us to do our regular $\Delta E - E$ particle identification

[2]We mentioned this effect in Chapter 2 for our carbon foils in the REX-beam-line.

6.1.2 A Solid State Detector

As mentioned already in the introduction to this section, stopping is due to interaction with electrons in the absorbing material, and as a result the incoming particle leaves a track of electron-hole pairs. The amount of electron-hole pairs created will depend on the strength of the stopping power, most pairs will be created where the stopping power is largest. Since the stopping power depends on particle charge and mass so will the distribution of electron-hole pairs.

Another point is that the amount of overall charge created when stopping a particle is proportional to the energy of the incoming particle, and (almost) independent of particle mass and charge. This is why we can calibrate a Si-detector with α-particles and then use that calibration for measuring e.g. proton energy. The "almost" in the previous statement is caused by the pulse height defect mentioned in chapter 3. In Silicon heavy particles produce slightly less electron-hole pairs than light ones. The difference between an α-particle and a proton is around 1%, and while the effect was already described in 1976 [31] a complete physics explanation has not yet been found. However, such an explanation must take into account the fraction of the energy loss going to nuclear collisions, as well as the effect of recombination among electron-hole pairs [74].

In order to extract the produced electron-hole pairs from the detector, we apply an electrical field, or biasing voltage. In an electrical field, electrons and holes will travel in opposite directions, but contribute to the same electrical signal. Since electrons and holes differ greatly in their physical representation,[3] the mobility of the two is not the same. For Silicon detectors the mobility of holes is around one third of the mobility of electrons, meaning that in the same electrical field electrons travels three times as fast though the detector as the hole.[4]

Collecting all the information from above we now reach the central point of this discussion: What influences the signal from the detector? We know that as soon as an ionizing particle hits our detector it will produce electron-hole pairs. Since our detector is biased these will start moving in opposite directions. A moving charge constitutes a current. This will be picked up by our preamplifier. Hence we have our detector signal.

The preamp connected to the detector acts as an integrator as well as an amplifier, summing up and amplifying individual charges. This means that the height of the preamp pulse is proportional to the total amount of charge created, and thereby to the incoming particle energy.[5] The time-scale

---

[3]The electron is a free particle while a hole is the absence of an electron from an atom.

[4]For completeness we should mention here that all the Silicon detectors we shall be working with are np-diodes, run with reverse bias and fully depleted to make the active detector region as large as possible, and to facilitate the charge collection. Since the details of this information is not central to this discussion, we refer to chapter 11 in [72] instead.

[5]Hence the term "Pulse-height defect".

for migration of an electron in our DSSSD detector is 10ns, meaning that traveling through 60μm of Silicon takes around 10ns. Once a charge, be it an electron or a hole, reaches the edge of the detector where our contacts are located, they stop contributing to the signal. The time from the beginning of the pulse and to its maximum is called the rise-time. Usually beginning and end is defined as 10% and 90% of the maximum height of the signal.

We now see that the shape of the detector signal is influenced greatly by a factor such as stopping depth, which in turn is influenced by particle charge and mass. If a particle stops close to an edge, it will generate the most charges close to that edge, and in turn will leave the majority of one set of charges with a relatively short path to travel while the other set will have a correspondingly longer one. If this can be resolved in our preamp we should see a sharp rise up to a certain height, naively around half of the total height, and then a flatter rise the rest of the way due to the longer migration time for the other charges. This effect should be more pronounced if the electrons are close to "home" while the holes have longer to travel.

Through this entire discussion we have assumed that no particles and no holes will be lost due to capture or recombination in the detector material. This is a good approximation as long as our heaviest particles are He-isotopes and our detector is only 60μm thick. For thicker or heavier particles, electron-plasma effects due to the intensity of ionisation in the detector makes this assumption invalid.

Armed with this knowledge we are now ready to move on to the experimentalists approach to the task.

6.2 Real world implementation

As mentioned in the beginning of this chapter there is a striking difference between describing a theoretical effect and actually constructing a system to try and measure it, let alone use it for something practical. The combination of pulse-height defect, straggling and dead-layer effects makes it less than obvious exactly how to differentiate signals from different particles, but this is our purpose.

The task of constructing an identification system was split up into various sub tasks. Firstly a system needed to be constructed to capture, digitize, and subsequently store individual pulses or waveforms. Secondly, analysis of these waveforms to determine which parameter(s), if any, can be used to distinguish different particles with the same energy.

The concept of identification rests on the assumption that the signal waveform is solely defined by particle and detector and not by the electronics between detector and digitization. Therefore, the preamplifier used in this project have to process the signal faster than the detector can discharge, so as not to distort the output by integrating the signal. This means that the

rise time of a preamp has to be of the order of a nano second.

Once a comprehensive knowledge is gained as to how the pulse shapes depend on particle types, and maybe on detector types, the third task is to devise a system for real-time particle identification. Firstly for one or two channels using existing electronics but the ultimate goal is to design a system capable of working with hundreds of channels in dedicated VME modules at a high count rate.

The two tasks we focused on during our work in Madrid was construction of the capturing system and preparation for online identification. The actual task of identifying features in individual spectra was put on hold until we had an idea of the nature of the effort that would be needed in this area.

6.2.1 Hardware

In setting up two such systems a wide range of equipment is needed. Here we discuss the essential parts of our set-up. Since the captured signal depends on both detector, preamp and in principle cabling, in order to make our work as generally applicable as possible, we tried to work with several components for each step. Throughout these efforts our particle sources were α-sources, similar to the ones used in the calibration of our DSSSDs. A more diverse supply of particles and energies was in theory available from CMAM, but not necessary for these first steps.

Detectors

On the detector side we used two planar Silicon detectors with thicknesses of 100μm and an active area of around 3cm^2. We also had a 16×16 60μm DSSSD, but unfortunately retrieving the signal from a single strip while putting bias on the entire DSSSD proved to be a very difficult task, and one that we did not solve at that time.[6] For that reason we only used the two much simpler planar detectors.

For the purpose of this thesis we focus our attention on particle identification in silicon detectors. Pulse Shape Analysis can also serve other purposes. Concurrently with the work being performed on Silicon, testing of the technique for use in CZT-detectors used in experiments looking for neutrino-less double β-decay [75] was performed as well . Since electron-hole mobility in a CZT-crystal is poor, PSA would enable corrections for interaction depth and thus improve energy resolution. We shall not comment any further on the CZT-portion of DLEP, but refer to the forthcoming thesis by John McGrath, University of York.

---

[6]The reason we needed the signal for only one strip is due to the other hardware introduced below.

Figure 6.6: Picture of LeCroy WavePro digitizer. From [76].

Pre amplifiers

As noted in the introduction to this section and in [67], the choice and construction of the preamp used for this type of study is very important for the quality of the information extracted about the detector signal. It is vital that the preamplifier is fast enough and has a low noise level so as not to disturb or distort the pulse shape coming from the detector.

The selection of Pre-amps we had access to included the family of Mesytec MPRs described in chapter 3, an old Ortec single channel preamp, and a single channel Ortec Fast Preamplifier 9326. Of these only the last one truly had the potential to deliver a usable particle-dependent signal, while the others were used for testing different parts of the setup.

Digitizers

The heart of our system, the key to particle identification, is the acquisition system. For our purpose such a system needs a fast Analog-Digital Converter (ADC) capable of capturing entire pulse shapes and a way of digitally storing, analyzing, and plotting these waveforms. The digitization needs to be fast enough to resolve slight differences in rise time, which means at least 3-4 measurements on that part of the signal.

Our Digitization system or DAQ is split into two separate units. The first one is a LeCroy WavePro 7000 DDA5005A Digital Oscilloscope, the LeCroy. This oscilloscope is capable of sampling signals at 40GSamples/s over 4 channels, corresponding to a 0.1ns time resolution, and can store the acquired waveforms. The scope is also a fully functional PC with many features to facilitate on-line data analysis. For instance, it is able to histogram data on the waveforms in real-time. Initial testing with this scope is ideal

Figure 6.7: Picture of the Acquiris digitizer crate with 440DC cards. From [77].

as it requires little programming in order to achieve its main functions. At the same time its sampling rate is faster than any other equipment we had access to, and it is therefore very useful as a tool to gain detailed knowledge about signal waveforms.

The main part of the second acquisition system was the Acquiris DC440 ADC, housed in crate as seen in figure 6.7. The Acquiris system consists of a fast ADC in the crate connected to a Linux PC by a dedicated PCI card. It is capable of sampling at a rate of 880MSamples/second over 2 channels, which is a factor of 25 slower than the LeCroy scope, giving it a time resolution of 2.3ns. The interface for the Acquiris system is based on C++ code and is thus completely customizable, but also rather complicated to work with under changing conditions. Once the different characteristics of particle waveforms are known from the initial tests, the Acquiris system will be used for our first attempt to perform on-line particle identification, even though it has this much slower sampling rate.

6.2.2 Software

A rather large set of programs and scripts had to be developed to handle several tasks. Simple things like plotting the acquired wave forms and extracting data like rise and fall time, to less simple tasks such as programming an interface for the Acquiris scope. We shall not go into specifics with the software here, but will try to highlight the contributions that were made in the section below.

6.3   Preliminary results

Being more or less the first people in our collaboration to have a stab at this task, we broke a lot of new ground, but also ran into a range of unforeseen incidents out of our control. Due to this progress on the project was slow and cumbersome and the limited advances that were made are hard to document.
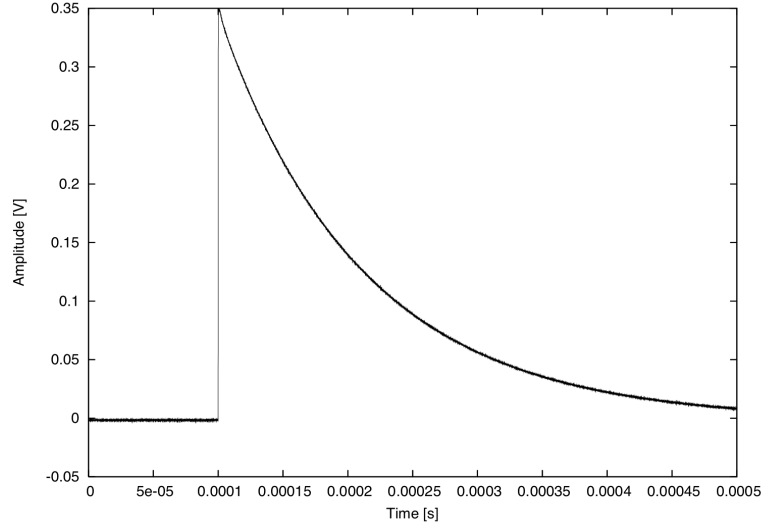
Figure 6.8: Figure of a single preamp pulse digitized with the Acquiris Digitizer

Nonetheless, the steps that were completed, while small, were necessary steps toward the end goal of identifying particles through PSA.

Before any attempt could be made to understand any signals or waveforms, the first step was to set up and configure the two waveform recording systems. While the LeCroy was rather simple to get up and running, the Acquiris system was a lot less so. In figure 6.8 one of the first preamp-pulses captured with the Acquiris system can be seen. This is from a standard Mesytec MPR-1 preamp. In the spectrum we have sampled the waveform 100.000 times and correspondingly the resolution is very impressive. What was not impressive was the Acquiris dead-time which, with 100.000 points, was of the order of a second! From the figure we see that the rise-time of the preamp is very fast, while the fall-time is around 400μs.

Having captured waveforms for both devices we constructed scripts and conversion software to enable plotting of the raw data that were dumped in two different ASCII-formats by the digitizers. Subsequently we made the first attempt to synthesize information from the spectra by automating calculation of rise- and fall-times, peak,and integral values. We were now ready to move on to the interesting preamplifier, the Ortec Fast Preamplifier 9326.

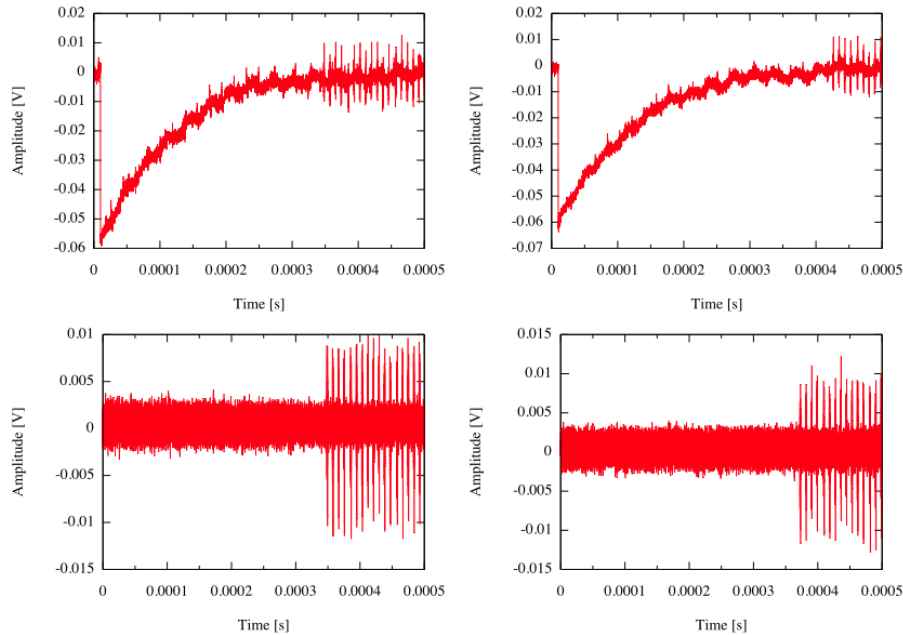This was a big disappointment. The Ortec was in theory both fast,

Figure 6.9: The top two panels show the signal from the doubly amplified signal from the fast Ortec Preamp. The bottom two show a random sampling of the noise in this setup

and powerful enough to yield at least a measurable signal in our digitizers. However, nothing could be seen above the noise. In our MPR-Pre-amps we saw signals around 400mV with the planar Si-detectors and our α-particles. Using a pulser we determined the MPR-Pre-amps to have an amplification of around 500, and our detector-signal was thus of the order 1mV. The Ortec specification was 20 times amplification, and this too was seen with a pulser. This gives a theoretical signal around 20mV, comparable to the noise level seen in our setup. Shortening cable lengths and using copious amounts of tinfoil we got our noise level down to 3mV, which should be enough to see a 20mV signal. Unfortunately this did not happen. The noise level can be seen in the two bottom panels of figure 6.9.

In a desperate move, the Fast Ortec was connected to an old fast amplifier with a 10ns rise-time. This combination yielded the two top panels of figure 6.9. To our delight we saw signals, meaning that something was coming through the Ortec. This meant, however that we could not see it in our digitizers. The extra amplification step left us with the original rise-time limitation of the MPR-Pre-amps. When comparing figure 6.9 to figure 6.8 we also see that we have a great deal more of noise picked up.

Several attempts to tin-foil our way out of the noise proved futile. Desperate attempts to use different sources provided no clear difference in wave-
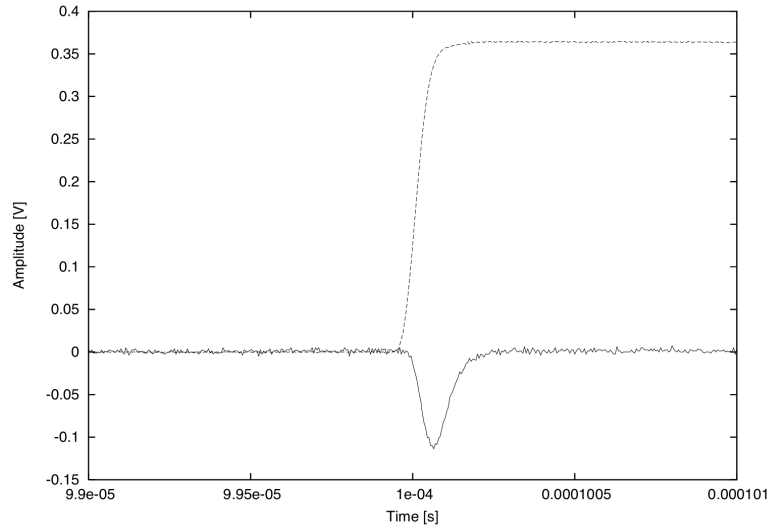
Figure 6.10: Figure showing a zoom of a pulse equivalent to the one in figure 6.8 but zoomed in on the rising portion of the signal. The bottom signal is the corresponding trigger signal from the shaper shown for comparison. The distance between ticks in the x-axis is 500ns.

forms, which would also have been surprising. Thus true attempts at PSA had to be put on hold. As an alternative strategy we looked for the fastest signal in our lab to try and do testing with that. The MPR-Pre-amps had a 10ns rise-time, so in theory digitizing this could allow us to test our equipment, but it turned out that the trigger-signals were usable too.

Figure 6.10 shows a zoom in on rise of a signal similar to that in figure 6.8. We see that the rise-time of the preamp signal is of the order of tens of ns. In the same figure we also see the trigger signal. It is clear that this signal can be fully digitized with a lot fewer points than the full waveform of the preamp pulse, and so we used this as a testing bed for some online calculations.

Unfortunately, no new faster and more powerful preamp could be acquired while we were in Madrid, and so our efforts were grounded to a halt at this stage.

6.4 The future of DLEP

The part of DLEP concerning PSA has more or less been in hibernation since the spring of 2007, when the Madrid team split up and went back to their separate universities. Test with new possibly faster preamps have been performed in Seville, but the results are still under analysis.

Due to this very limited experience with pulse shapes we are unable to say that the efforts in all cases will be worthwhile. A set of fast Pre-amps and a way to extract signals from our DSSSDs, would be a couple of very nice steps on the way to completion of this task.

One thing we have not mentioned is the possibility of comparing front and back side signals for our DSSSDs. Since signal is extracted from both sides, differences in signal timing or possibly shape may hold identifying features. This possibility is unique to these double-sided detectors and has not been tried before. This should definitely be tested once the appropriate equipment is available.

The status of the other part of DLEP, the monolithic detector, was more or less covered in the introduction of this chapter. For this detector we also need further studies to understand exactly what is going on inside the detector, before it can be used in nuclear physics experiment.

Chapter 7

Summary and Outlook

The pioneering study of the reaction ^{11}Be+d at an ISOL facility presented in this thesis yielded several results. We successful showed significant feeding to several interesting regions, although not with sufficient resolution to separate individual states in most cases. We fully expect to be able to extract structure parameters in the final analysis.

Furthermore the success of this experiment allows us to plan the next step which will add γ-detection to the setup to greatly improve resolution.

On the DLEP-project we have started work that will hopefully lead to the development of online identification of charged particles at much lower energies than possible with traditional techniques. We have taken the first steps towards analyzing and identifying charged particles based on the pulse shape of the signal generated when stopped in a thin silicon detector.

7.1 Outlook for low energy Be-reactions

As already mentioned, the next step for this reaction at ISOLDE will be to add the Mini-ball 4π γ-detector to the setup.

A second improvement should be a higher beam energy available at REX. Our current experiment was run at 2.25MeV/u due to an under-dimensioned amplifier for the last 9-gap resonator in the REX linac. This has now been rectified, and so we expect to get the full 3.1MeV/u for reactions.

Also we expect a higher yield of ^{11}Be, since the yield at the last experiment was unnaturally low out of ISOLDE compared to previously seen values, and this should give us significantly better statistics. We also aim for better angular coverage, and at more extreme angles, to see the interesting parts of the angular distribution of the charged particles. We hope to not again be hindered by a broken detector, and better detector coverage should also improve our statistics.

Not many places are able to produce low energy ^{11}Be beams. We are therefore at this time almost the only ones exploring these isotopes at low

energies. The only other facility able to produce and deliver ^{11}Be-beam in the near future, at a quality as good or better than ISOLDE is TRIUMF in Vancouver, Canada. For the time being we do not know of similar activities yet at that facility.[1]

7.2 The future of REX- and ISOLDE

The not so distant future of our reaction experiments with light nuclei is very closely tied to the only facility in Europe that can deliver them at low energies, REX-ISOLDE. While small scale collaboration with TRIUMF in Vancouver is under way, the main focus of our reaction studies for the foreseeable future will still be at ISOLDE. For that reason we take a look at the future of ISOLDE and REX-ISOLDE.

The main focus of the entire CERN organization is currently to get the Large Hadron Collider (LHC) online. Since ISOLDE is an integrated part of the CERN accelerator structure, a direct effect of this will be a reduction of the amount of protons dedicated to ISOLDE. Fewer protons will give fewer radioactive nuclei and thus less intense ISOLDE beams. This is not a major issue since ISOLDE is still guaranteed 30-40% of the total proton pulses. Furthermore, the LHC upgrade includes a planned intensity upgrade of a factor of three in 2013. A more significant effect felt indirectly is that LHC is attracting most of the available CERN resources, making it difficult for small scale facilities like ISOLDE to get e.g. technical assistance.

A lot of changes are planned for the future of ISOLDE, most of them in connection with the High Intensity and Energy (HIE) upgrade of the facility. The technical side of this upgrade has been thoroughly treated in [78] and we shall mention only some of the interesting points here.

Target and ion-source development is, as mentioned in chapter 2, a major priority at ISOLDE and one of the reason the facility is so successful. The future program will continue this development, among other things with a new target handling system. Also a significant upgrade of the RILIS laser ion-source will take place. This upgrade has already started with the installation of new YAG-driver lasers and will be followed by an upgrade from two Dye Lasers to three Solid State Lasers enabling an even more selective ionisation. In connection with the RILIS upgrade an offline laser lab for development work will allow for better usage of the new RILIS.

Continuing from the ion-source in the same fashion as in chapter 2 a new HRS magnet is planned to replace the current out-dated model. This should significantly improve mass resolution.

On the REX-side several major improvements are planned. One of the major upgrades is an improved EBIS ion-source with a breading time four times as fast as the current version. This should allow for less decay loss

---

[1]But we are beginning to hear rumors...

in this step of the process. A new ECR ion-source is also planned. This ion-source would have a significantly higher breading time than EBIS, but would add CW operation as an option, instead of the pulsed structure of EBIS.

The REX-linac is also in for an upgrade that will proceed in three steps. The first will be an upgrade on the existing, now extended, beam-line to allow acceleration up to 5.5MeV/u. A later second major upgrade could allow for acceleration up to 10MeV/u. For both upgrades a super conducting linac is currently recommended. A possible third step would be to add a deceleration component after REX in order to do reactions at astrophysical energies.

The upgrades of both EBIS and the linac should give much more well-defined beam characteristics in the form of smaller longitudinal and transverse beam emittance. Together with the ISOLDE upgrades, this should give more intense beams and beams of more nuclei than is possible today, significantly pushing the limits of the kind of physics study that can be done at ISOLDE.

A full review of the physics possibilities with a fully implemented HIE-ISOLDE has been examined in [79] and we shall only mention a few here. Obviously the simple fact that more isotopes will be available to study opens up all kinds of opportunities.

The higher beam energy of REX will also bring significant improvements to many areas. For nuclear physics it will allow reactions close to the coulomb barrier for significantly heavier nuclei than is currently possible. Decay studies can also benefit from the upgraded REX since implantation decay tagging experiments should now become possible.

The structure studies performed by our group and at the Mini-ball facility, should also benefit greatly since transfer reactions to more exotic nuclei, and more exotic states in currently available nuclei, will become possible. Higher energy should also mean higher cross-sections and detection efficiency since we will be able to cover more angles with the same detectors. As a final benefit, spectroscopic factors will become less model-dependent at higher energies, and so structure information should be more easily accessible.

7.3 Future Experimental Nuclear Physics

Experimental nuclear physics, and more than anything front-line experimental nuclear physics, is to a large extent if not driven then at least confined by the available experimental equipment. This is both on detector and the production/accelerator side. For the same reason, pushing the limits of our knowledge of nuclear physics requires us to push existing equipment or to develop entirely new hardware. We have seen this in this thesis with DLEP, and with HIE-ISOLDE above, but of course a lot of other developments are

going on around Europe.

A number of small scale facilities are used by our group mainly for decay studies and simple reactions. These include JYFL in Finland, KVI in the Netherlands and CMAM in Spain. All of these facilities are continually upgrading their capabilities and we will not cover these in any detail here.

A number of very exciting large scale facilities are either under construction or under planning and will determine the reaches of European nuclear physics in the next 15-20 years. We will try to give a short summary below.

7.3.1 Large Scale Facilities

The not too distant future will see two new and exciting large scale facilities come online. Both of these will deliver beams at significantly higher energies than ISOLDE, and both have very promising complementary physics perspectives. The two facilities, SPIRAL II at GANIL in France, and FAIR placed at GSI in Germany, promises to significantly push the limits of what kind of nuclear physics experiments can be done. We will spend a few words on these two, and on the far future project EURISOL which has 10-15 years until construction and has yet to be finalized.

SPIRAL II

SPIRAL II [80] is the upgrade of the already excising French facility SPIRAL at GANIL. Though it is mostly a French project, access to the facility is open and many international collaborations work at the facility. SPIRAL uses a sequence of cyclotrons to accelerate a beam of radioactive nuclei to tens of MeV/u. Though rather large, it is the smallest facility of the three we mention here.

The upgraded SPIRAL II will produce radioactive nuclei using a range of well known techniques including ISOL and in-flight methods. The goal is to optimize the process for each nucleus under investigation. SPIRAL II will be able to deliver beams in broad areas of the nuclear chart and the beam energy will be up to 25MeV/u.

While SPIRAL II will focus its activities on nuclear physics, it will be open to other branches of physics such as material science and atomic physics. Also SPIRAL II collaborates with FAIR on technology transfer and detector development to maximize the usage of both.

SPIRAL II will serve a physics community of around 700 physicists, the same number as GANIL currently serves using SPIRAL. The first ISOL beam from SPIRAL II is scheduled to be at available by 2013.

FAIR

The planned Facility for Anti-Proton and Ion Research [81] will be a unique facility in the world. It will be able to utilize both regular matter and

anti-protons in a very wide range of experiments.

Technically the facility will be very complex with several ring-structures, a double synchrotron, a fragment separator, as well as cooling rings and several very large detector setups. A project of this scale requires international cooperation and although the German government bears the brunt of the cost (3/4), a group of 15 countries have so far agreed to contribute money and equipment to the facility. Like SPIRAL II it will be open to researchers from other countries as well.

The revolutionary design will allow several experiments to be run in parallel, even though there will be only one driver accelerator. This will maximize the usage of the facility.

FAIR will impact a wide range of physics fields, from the search for super-heavy nuclei and high density matter, to reactions at astrophysical energies. Eventually this facility will be able to do it all. The availability of anti-protons will revolutionize nuclear structure research since it will allow interaction between exotic nuclei and anti-protons, which has never before been done.

Also applied physics research will take place at FAIR that could potentially impact such diverse areas as fusion power and cancer treatment

The first stage of FAIR should be ready in 2013, while the entire facility should be complete around 2016. Up to 3000 physicists will be working at FAIR, which is half the number working at CERN.

EURISOL

The final facility we mention is EURISOL [82]. This is a project that is still in the planning phase and no decision has been taken on e.g. location. However, some general physics issues have been clarified in an enormous amount of paperwork and a large number of meetings. EURISOL will be a joint European research facility with unique and ground-breaking capabilities. The main feature of the EURISOL design is a 5MW target station for neutron conversion. This will be used for uranium fission reactions. Together with three 100kW stations and the ISOL separation method, this will give access to unprecedented intensities of exotic nuclei. As an example secondary fragmentation of ^{132}Sn could reach completely unexplored areas in the nuclear chart.

EURISOL is meant to complement and expand on the capabilities already present in Europe with ISOLDE, SPIRAL II and FAIR. Already the EURISOL user groups [83] are sharing knowledge and ensuring technology transfer between the existing facilities and EURISOL. As an example the target development that is being made for EURISOL is directly applicable at ISOLDE.

7.4   Final words

In the introduction I mentioned the question of whether everything was know in nuclear physics. To the initiated reader, it should be clear by now that this is not at all the case. The facilities discussed above will make sure that nuclear physics discoveries will continue to be made far into the future.

Bibliography

[1] Chris Guy and Dominic Ffytche, An Introduction to The Principles of Medical Imaging, Imperial College Press, 2005

[2] J. Gilles, CERN Courier, Nov. 27, 1998

[3] W. Rom *et al.*, Radiocarbon 41 (1999) 183

[4] C. Holden, Science 30 (2003) 759

[5] G. R. Satchler, Introduction to Nuclar Reacions, Second Ed., MacMillian Education Ltd., 1990

[6] P. E. Hodgson, E. Gadioli and E. Gadioli Erba, Introductory Nuclear Physics, Oxford University Press, 1997

[7] J. Chadwick, Proc. Roy. Soc. A 136 692

[8] N. Bohr, Nature 137 (1936) 344

[9] Steven C. Pieper Nucl. Phys. A 751 (2005) 516c

[10] A. S. Jensen *et al.*, Rev. Mod. Phys. 76 (2004) 215

[11] B. M. Sherrill, Science 320 (2008) 751

[12] I. Tanihata *et al.*, Phys. Rev. Lett. 55 (1985) 409

[13] P. G. Hansen and B. Jonson, Europhys. Lett. 4 (1987) 409

[14] H. L. Ravn, Phil. Trans. R. Soc. Lond. A 356 (1998) "Radioactive ion-beam procects based on the two-accelerator or ISOL-principle"

[15] H. Geissel, G. Münzenberg, K. Riisager, Ann. Rev. Nucl. Sci. 45 (1995) 163

[16] E. Kugler *et al.*, Nucl Instr. and Meth. B 70 (1992) 41

[17] B. Jonson and A. Richter, Hyperfine Interactions 129 (2000) 1

[18] U. Köster, Radiochim. Acta 89 (2001) 749

[19] C. Catherall *et al.*, Rev. Sci. Instrum. 75 (2004) 1614

[20] U. Köster *et al.*, Hyperfine Interactions 127 (2000) 417

[21] H. B. Jeppsen *et al.*, Nucl. Phys. A748 (2005) 364

[22] D. Habs *et al.*, Hyperfine Interactions 129 (2000) 43

[23] P. Schmidt *et al.*, Nucl. Phys. A 701 (2002) 550c

[24] F. Wenander *et al.*, AIP Conference Proceedings 572 (2001) 59

[25] R. Rao *et al.*, Nucl. Phys. 427 (1999) 170

[26] T. Sieber *et al.*, Nucl Phys. A 701 (2002) 656c

[27] H. Podlech T. *et al.*, Nucl Phys. A 701 (2002) 651c

[28] ISOLDE homepage: `http://isolde.cern.ch`

[29] U. C. Bergmann, H. O. U. Fynbo and O. Tengblad, Nucl. Instr. and Meth. A 515 (2003) 458

[30] O. Tengblad *et al.*, Nucl. Instr. and Meth. A 525 (2004) 657

[31] J. B. Mitchell, S. Agami and J. A. Davies, Radiation Effects Vol. 28 (1976) 133

[32] Haakan T. Johansson, Licentiate thesis, Chalmers University of Technology (2006) Unpublished

[33] O. Niedermaier *et al.*, Phys. Rev. Lett. 94 (2005) 072501

[34] H. B. Jeppesen *et al.*, Phys. Lett. B 642 (2006) 449

[35] R. Anne *et al.*, Nucl. Phys. A 575 (1994) 125

[36] T. Nakamura *et al.*, Phys. Lett. B 331 (1994) 296

[37] T. Aumann *et al.*, Phys. Rev. Lett. 84 (2000) 35

[38] M. Chartier *et al.*, Phys. Lett. B 510 (2001) 24

[39] J. S. Winfield *et al.*, Nucl. Phys. A 683 (2001) 48

[40] P. Palit *et al.*, Phys. Rev. C 68 (2003) 034318

[41] J. A. Tostevin *et al.*, Phys. Rev. C 66 (2002) 024607

[42] A. Shrivastava *et al.*, Phys. Lett. B 596 (2004) 54

[43] F. Barker, J. Phys. G 2 (1976) L45

[44] A. Navin *et al.*, Phys. Rev. Lett. 85 (2000) 266

[45] M. Freer *et al.*, Phys. Rev. Lett. 82 (1999) 1383

[46] M. Freer *et al.*, Phys. Rev. C 63 (2001) 034301

[47] Y. Kanada-Enyo and H. Horiuchi, Phys. Rev. C 68 (2003) 014319

[48] T. Suzuki *et al.*, Phys. Rev. C 67 (2003) 044302

[49] G. Martinez Pinedo *et al.*, Private Communication 2004

[50] A. Bonaccorso and N. Vinh Mau, Nucl. Phys. A 615 (1997) 245

[51] F. M. Nunes *et al.*, Nucl. Phys. A 703 (2002) 593

[52] E. Garrido *et al.*, Phys. Lett. B 600 (2004) 208

[53] C. Romero-Redondo *et al.*, Phys. Lett. B 660 (2008) 32

[54] H. T. Fortune, G.-B. Liu and D. E. Alburger, Phys. Rev. C50 (1994) 1355

[55] S. Shimoura *et al.*, Phys. Lett. B560 (2003) 31

[56] H. Iwasaki *et al.*, Phys. Lett. B491 (2000) 8

[57] S. Shimoura *et al.*, Phys. Lett. B654 (2007) 87

[58] Antonio M. Moro Muños, Private Communication

[59] M. V. Andrés *et al.*, Proposal to ISOLDE-NToF Committee, CERN-INTC/2006-010

[60] V. Lapoux *et al.*, Phys. Lett. B 658 (2008) 198

[61] A. M. Sánchez-Benítez *et al.*, Nucl. Phys. A 803 (2008) 30

[62] F.Ajzenberg-Selove, Nucl. Phys A 506 (1990) 1

[63] D.R. Tilley *et al.*, Nucl. Phys A 745 (2004) 155

[64] JRA-4 Eurons Proposal, DLEP

[65] S. Tudesco *et al.*, Nucl Instr. and Meth. A 426 (1999) 436

[66] C. A. J. Ammerlaan *et al.*, Nucl Instr. and Meth. 22 (1963) 189

[67] H. Hamrita et al., Nucl Instr. and Meth. A 531 (2004) 607

[68] L. Bardelli *et al.*, Nucl Instr. and Meth. A 560 (2006) 517

[69] J. Eberth and J. Simpson, Prog. Part. Nucl. Phys. 60 (2008) 283

[70] L. Bardelli *et al.*, Nucl Instr. and Meth. A 521 (2004) 480

[71] L. Bardelli *et al.*, Nucl. Phys A 746 (2004) 272c-276c

[72] G. F. Knoll, Radiation Detection and Measurement Third Ed., John Wiley and Sons, 2000

[73] `http://commons.wikimedia.org`

[74] T. D. M. Weijers *et al.*, Nucl. Instr. Meth. B 190 (2002) 387

[75] K. Zuber, Contemporary Physics 45 (2004) 491

[76] LeCroy company website: `http://www.lecroy.com`

[77] Agilent Technologies company website: `http://www.acquiris.com`

[78] M. Lindroos and T. Nilsson, HIE-ISOLDE: The technical options, CERN-2006-013

[79] K. Riisager *et al.*, HIE-ISOLDE: The scientific opportunities, CERN-2007-008

[80] SPIRAL II website: `http://www.ganil.fr/research/developments/spiral2/`

[81] FAIR website: `http://www.gsi.de/fair/`

[82] EURISOL website: `http://www.eurisol.org`

[83] EURISOL User Group website: `http://www.eurisol.org/usergroup/`